A NMR and molecular dynamics study of CO2-bearing basaltic melts and glasses

Yann Morizet, R. Vuilleumier, M. Paris

A NMR and molecular dynamics study of CO_2-bearing basaltic melts and glasses

Y. Morizet [a,b,*], R. Vuilleumier [c], M. Paris [d]

[a] CNRS/INSU-Université d'Orléans — BRGM, UMR 7327, Institut des Sciences de la Terre d'Orléans, 1a rue de la Férollerie, 45071 Orléans, France
[b] Université de Nantes, Nantes Atlantique Universités, Laboratoire de Planétologie et Géodynamique de Nantes (LPGN), UMR CNRS 6112, 2 rue de la Houssinière, 44322 Nantes, France
[c] Laboratoire PASTEUR, Département de Chimie, Ecole Normale Supérieure et Université Pierre et Marie Curie (Paris 6), UMR CNRS 8640, 24 rue Lhomond, 75005 Paris, France
[d] Institut des Matériaux Jean Rouxel (IMN), Université de Nantes, UMR CNRS 6502, 2 rue de la Houssinière, BP32229, 44322 Nantes Cedex 3, France

ARTICLE INFO

Article history:
Accepted 23 March 2015
Available online xxxx

Keywords:
CO_2 speciation
Aluminosilicate network speciation
High temperature melt *versus* glass
MAS NMR
First-principles molecular dynamics simulations

ABSTRACT

The presence of volatile, especially carbon dioxide (CO_2), in silicate liquids is considered as a key parameter to magmatic degassing and eruptive processes. Unfortunately, due to experimental difficulties, our current knowledge on the CO_2 effect on silicate melt structure is weak and relies on the observation of *ex-situ* recovered CO_2-bearing glasses.

In the present work, we confront the results obtained from NMR spectroscopic observations of glass synthesised at pressure between 0.5 and 3.0 GPa and theoretical investigations from first-principles molecular dynamics (FPMD) simulations conducted at 5.0 and 8.0 GPa on high temperature melt for a simplified basaltic composition. The results obtained on the aluminosilicate framework (molar fraction of silicon species and Al average coordination number) suggest that both *ex-situ* and *in-situ* results compare adequately. The results are in agreement with our current knowledge on the change in aluminosilicate melt/glass structure with changing intensive conditions. Increasing pressure from 0.5 to 8.0 GPa induces 1) an increase in the average Al coordination number from 4.1 to almost 5.0 and 2) an increase in the degree of polymerisation with NBO/Si changing from 1.30 to 0.80. The presence of CO_2 does not seem to induce a dramatic change on both the average Al coordination number and the NBO/Si. FPMD simulations performed with 0 and 20 wt.% CO_2 at 8.0 GPa result in a change from 4.84 to 4.96 for the average Al coordination number and in a change from 0.87 to 0.80 for the NBO/Si value, respectively.

On the contrary, there is a lack of consistency in between the CO_2 speciation obtained from NMR spectroscopy and from FPMD simulations. Whereas the analysis of glasses does not reveal the presence of CO_2^{mol} species, the FPMD simulation results suggests the existence of a small proportion of CO_2^{mol}. Further work with *in-situ* experimental approach is therefore required to explain the observed lack of consistency between the CO_2 speciation in glass and in high temperature melt with basaltic composition.

1. Introduction

Fluids and melt are ubiquitous materials within the Earth deep interiors. After water, carbon dioxide (CO_2) is the second most important volatile involved in magmatic systems (Gerlach and Graeber, 1985; Jambon, 1994; Symonds et al., 1994; Morizet et al., 2002, 2010) and in some volcanic systems CO_2 becomes the dominant one (Holloway, 1981; Giggenbach, 1997; Andersen and Neumann, 2001; Massuyeau et al., submitted for publication, in this issue). Its impact on magmatic processes is now well-recognized (Eggler, 1974; Brey and Green, 1975, 1976; Wallace and Green, 1988; Falloon and Green, 1989; Draper and Green, 1997). Owing to the large amount of experimental investigations since decades, CO_2 solubility and speciation are currently well-constrained as a function of composition (Fine and Stolper, 1986; Pan et al., 1991; Dixon, 1997; Papale, 1999; Botcharnikov et al., 2005, 2006; Iacono-Marziano et al., 2008; Shishkina et al., 2010; Iacono-Marziano et al., 2012; Morizet et al., 2014a) and intensive parameters (Blank and Brooker, 1994; Dixon et al., 1995; Morizet et al., 2002; Newman and Lowenstern, 2002; Behrens et al., 2009; Lesne et al., 2011; Iacono-Marziano et al., 2012).

However, one of the major deficiencies of our current knowledge of CO_2 behaviour in aluminosilicate compositions is that most of the available information on CO_2 speciation is based on the study of *ex-situ* recovered samples quenched to glasses. It appears problematic because recent investigations showed that the CO_2 speciation recorded in glasses cannot unambiguously be applied to a corresponding high temperature melt condition (Morizet et al., 2001; Nowak et al., 2003; Spickenbom et al., 2010). The CO_2 speciation is suggested to be decoupled from the aluminosilicate network speciation. At temperature

* Corresponding author at: Laboratoire de Planétologie et Géodynamique de Nantes (LPGN), Université de Nantes, CNRS/INSU — UMR CNRS 6112, 2 rue de la Houssinière, BP 92208, 44322 Nantes Cedex 3, France. Tel.: +33 2 5112 5491; fax: +33 2 5112 5268.
E-mail address: yann.morizet@univ-nantes.fr (Y. Morizet).

below the glass transition, the silicate network speciation is fixed but CO_2 speciation still evolves. The results from Nowak et al. (2003) conducted on dacite and albite compositions (Fig. 1A) suggest that at high temperature in the melt, part of the CO_2 speciation is represented by CO_2^{mol} species formed through the following interconversion reaction governed by an equilibrium constant (K) between a carbonate group (CO_3^{2-}) and a CO_2 molecule (CO_2^{mol}):

$$CO_c^{mol} + O^{2-} \overset{K}{\leftrightarrow} CO_3^{2-}. \quad (1)$$

The interconversion reaction in Eq. (1) is probably oversimplified. The nature of the involved oxygen from the melt (O^{2-} in Eq. (1)) is currently unknown, (*i.e.* the negative charge distribution around the oxygen atom is not asserted and the surrounding cation is variable in nature). Those pioneer works (Morizet et al., 2001; Nowak et al., 2003) have focussed on simple compositions in which both C species (CO_2^{mol} and CO_3^{2-}) are present initially in the glasses.

For basalt-like composition in which CO_2 is dissolved solely as CO_3^{2-} groups, we currently do not have solid evidence of such an interconversion mechanism at high temperature in the melt. However, recent molecular modelling conducted by Guillot and Sator (2011) on simple haplo-basaltic composition (MORB) invoked a similar mechanism. As shown in Fig. 1B molecular dynamics simulation results on MORB under high temperature melt conditions conducted at 2273 K show that the proportion of CO_2^{mol} is gradually increasing with decreasing pressure (up to 70% CO_2^{mol} in relative to the total C species at 2.0 GPa). Guillot and Sator (2011) also showed that the proportion of CO_2^{mol} is strongly temperature dependent: 70% and 37% CO_2^{mol} at 2273 and 1473 K, respectively. Those results are in agreement with our current view of the interconversion between CO_2^{mol} and CO_3^{2-} groups observed in more acidic compositions (Morizet et al., 2001; Nowak et al., 2003). Nevertheless, it has never been witnessed experimentally for basaltic compositions in which the CO_2 speciation is only represented by CO_3^{2-} groups (*e.g.* Fine and Stolper, 1986; Pan et al., 1991; Pawley et al., 1992; Dixon et al., 1995; Morizet et al., 2010).

The molecular structure of aluminosilicate glass/melt can be approximated by a combination of several individual structural units, called Q-species (*e.g.* Grimmer et al., 1984; Brandiss and Stebbins, 1988; Merzbacher et al., 1990; Stebbins, 1995; Mysen and Richet, 2005) where Q represents a SiO_4 tetrahedron and is considered as a network forming unit. The notation Q^n is often employed where n represents the number of bridging oxygen (BO) per tetrahedron.

In complex aluminosilicate melts, Al^{3+} is also considered as a network forming cation (AlO_4 tetrahedra) whereas other cations (for example, Ca^{2+}, Mg^{2+}, Na^+ and K^+) are either network modifiers or charge balancing cations (*e.g.* Neuville and Mysen, 1996; Lee and Stebbins, 2000).

The way the different Q^n species combines within a silicate glass/melt has been extensively addressed. Early work by Mysen and co-workers based on micro-Raman spectroscopy (Mysen and Virgo, 1980; Mysen et al., 1980; Mysen and Frantz, 1994; Mysen, 1997) clearly established that several Q^n species are in equilibrium in the glass such as:

$$2Q^n \leftrightarrow Q^{n+1} + Q^{n-1} \quad n = 1,\ 2 \text{ or } 3. \quad (2)$$

Similar conclusion was also drawn from NMR investigations (Maekawa et al., 1991; Maekawa and Yokokawa, 1997; Zhang et al., 1997; Schneider et al., 2003; Xue and Kanzaki, 2004; Malfait et al., 2007a; Davis et al., 2011; Morizet et al., 2014b) for various types of compositions from simple binary M_nO–SiO_2 systems but also for more complex Al-bearing systems. This reaction implies that for a given chemical composition three Q-species are in equilibrium in glasses. The equilibrium in Eq. (2)provides also a view of the degree of polymerisation of a silicate glass/melt. This degree of polymerisation obtained by the Q-species distribution is dependent on the chemical composition and is commonly expressed by the NBO/T parameter which corresponds to the ratio between the non-bridging oxygen and the tetrahedra (Mysen, 1988, 1990). The NBO/T can be readily calculated from the concentrations of oxides. It is commonly assumed that for a $0.1 < NBO/T < 1$ calculated from the chemical composition, the reaction given in Eq. (2) involves Q^4, Q^3 and Q^2 such as:

$$2Q^3 \leftrightarrow Q^4 + Q^2. \quad (3)$$

This situation is of particular interest in the present study as the NBO/T is very close to one for the investigated composition (see Section 2).

From a general stand point, the molecular structure (Q^n distribution) of a high temperature melt is different from the one of the corresponding glass (Stebbins and Xue, 2014). The glass transition temperature (Tg) (Moynihan et al., 1976) separates the glassy state, with a frozen-in molecular structure, from the liquid state in which molecular

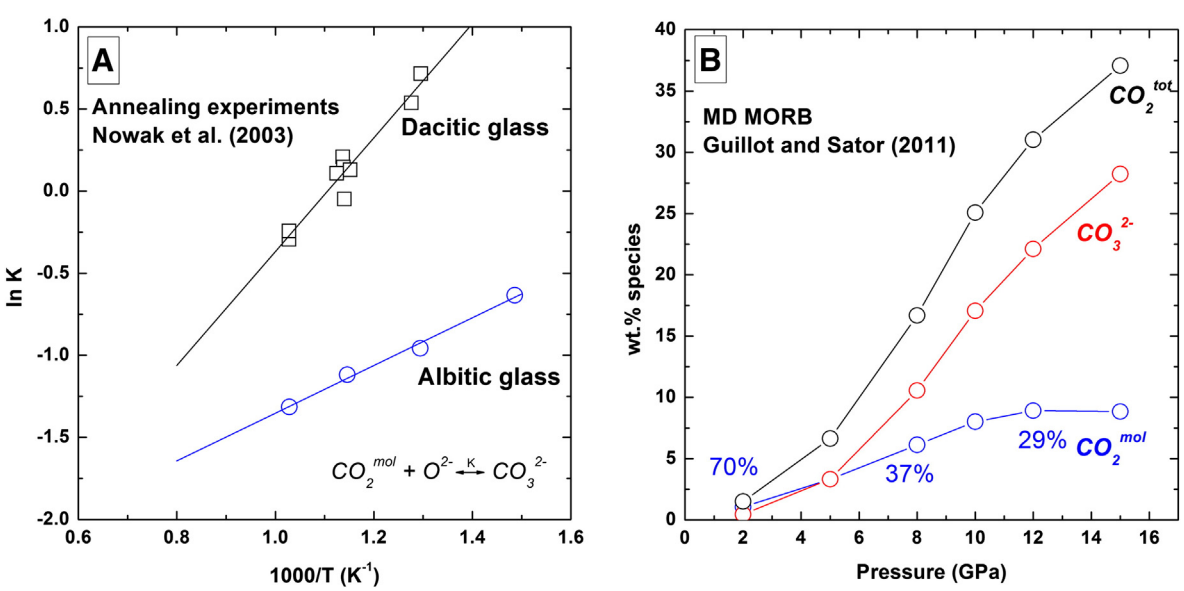

Fig. 1. A) Evolution of the equilibrium constant (K) for the interconversion reaction between CO_3^{2-} and CO_2^{mol} from annealing experiments of Nowak et al. (2003) on albitic and dacitic compositions. B) CO_2 solubility (CO_2^{tot}) and speciation (CO_2^{mol} and CO_3^{2-} groups) in MORB as a function of pressure (up to 15 GPa) derived from classical molecular dynamics simulations from Guillot and Sator (2011). Both studies imply the existence of a non-negligible abundance of CO_2^{mol} at high temperature in the melt.

structural changes are fast (Dingwell, 1995; Webb, 1997). The molecular structure preserved in a glass represents the molecular structure of an equivalent melt held at Tg.

Based on *in-situ* spectroscopic methods conducted at ambient pressure, previous works (*e.g.*Stebbins and Farnan, 1992; McMillan et al., 1994; Mysen and Frantz, 1994; Neuville and Mysen, 1996; Maekawa and Yokokawa, 1997; Malfait et al., 2007a,b) have shown that Al speciation (*i.e.* Al coordination number) and Q^n distribution are different in the high temperature melt (above Tg) and in the glass (frozen-in at Tg). Spectroscopic investigations on glasses with various fictive temperatures (almost equivalent to Tg; Tropin et al., 2011) showed comparable results: Al coordination number, concentration of non-bridging oxygens (NBO) and Q^n distribution slightly vary with varying fictive temperature (*e.g.* Brandiss and Stebbins, 1988; Stebbins et al., 2008; Thompson and Stebbins, 2013). However, there has been up to now a lack of structural information on volatile-bearing silicate melts at high pressure and high temperature. Mysen and Yamashita (2010) and Mysen (2012, 2013) recently addressed this problem; however those studies only considered simple compositions in the Na_2O–SiO_2 system in equilibrium with C–H–O fluid phase.

Experimental difficulties, including the temperature limitation in diamond anvil cell experiments, prevent the molecular structure to be investigated in complex melts such as basalt. One way to circumvent these experimental difficulties is to investigate the high temperature melt structure through molecular dynamics simulations, which have been routinely applied to investigate liquid properties in various systems (Belonoshko, 1994; Belonoshko and Dubrovinsky, 1996; Guillot and Sator, 2007a,b). More specifically, molecular simulation methods have been employed successfully to evaluate high temperature silicate melt thermodynamic, physical properties (Guillot and Sator, 2007a,b) and more recently CO_2-bearing silicate melt physical properties (Guillot and Sator, 2011). First-principles molecular dynamics simulations (Car and Parrinello, 1985; Vuilleumier, 2006), which rely on forces computed on the fly through density functional theory, allow to study melts at extreme conditions where the local environment can differ significantly from ambient conditions (Vuilleumier et al., 2009; Karki and Stixrude, 2010). The excellent agreement in between the measured and modelled silicate melt physical properties demonstrates the applicability of molecular dynamics methods for the description of silicate materials under *in-situ* conditions (Guillot and Sator, 2011; their Fig. 12 for CO_2 diffusion coefficient).

In the present work, we combine the two approaches to investigate the molecular structure of CO_2-bearing haplo-basaltic melt/glass composition: 1) first-principles molecular dynamics (FPMD) simulations will be used as a model for the basaltic melt under high temperature high pressure conditions relevant to the Earth mantle conditions; 2) nuclear magnetic resonance spectroscopic methods will be used to investigate the molecular structure of recovered basaltic glasses. One of the objectives of the present study is to find out if the recorded aluminosilicate structure in *ex-situ* glasses can be correlated to the one observed under *in-situ* conditions in the high temperature melt. The second objective is to find out if the CO_2 speciation in the high temperature basaltic melt is comparable to the CO_2 speciation recorded at the glass transition temperature. In particular, we will question the importance of CO_2^{mol} as a component of the complex haplo-basaltic melt at high temperature.

2. Experimental procedures and theoretical calculation methods

2.1. Sample synthesis

A synthetic haplo-basaltic (basG) composition in the CaO–MgO–Al_2O_3–SiO_2 system was prepared from a mixture of oxides (MgO, Al_2O_3 and SiO_2) and carbonate ($CaCO_3$). The oxides were dried in a box furnace at 1100 °C for several hours prior to mixing all oxides and carbonates together in an agate mortar. The $CaCO_3$ is also the source of CO_2 during the experiments and corresponds to 12.8 wt.% CO_2. Under the investigated experimental conditions (see below and Table 1), the initial 12.8 wt.% CO_2 is well-above the expected CO_2 solubility. The carbonate was added as 100% $Ca^{13}CO_3$ for ^{13}C NMR analyses. The SiO_2 was added as both $^{28}SiO_2$ and $^{29}SiO_2$ for ^{29}Si NMR analytical purpose. The calculated enrichment is ~70% ^{29}Si.

The composition was prepared so as to match the composition used in the FPMD simulations (see Section 2.3). The major element theoretical composition is reported in Table 1 on a CO_2-free basis: 48.87 wt.% SiO_2, 17.40 wt.% Al_2O_3, 16.33 wt.% CaO and 17.40 wt.% MgO. The initial composition has a NBO/T of 0.957 corresponding to a slightly depolymerised composition. The Al/Si ratio in the composition is 0.42. In the remaining of the manuscript, we will refer to both the NBO/T and the NBO/Si. The NBO/Si is calculated from the chemical composition but without taking into account the Al^{3+} concentration in the tetrahedral charges and only Si^{4+} is considered. The NBO/Si is of practical use as the theoretical value can be readily compared with the value derived from the ^{29}Si NMR spectra deconvolution (see Section 4.1.1). In the studied composition, the calculated NBO/Si is 1.358.

We conducted the high-pressure experiments in an end-loaded piston-cylinder apparatus following the method reported in Morizet et al. (2002). The experimental conditions are reported in Table 1: the pressure range is 0.5 to 3.0 GPa, the temperature range is 1773 to 1873 K. The temperatures were monitored by a WRe_3–WRe_{25} thermocouple in all experiments. The capsule was surrounded by an alumina sleeve to avoid contact with the graphite furnace.

For the experiments between 0.5 and 2.0 GPa, a 19 mm talc–Pyrex assembly was used. A tapered graphite furnace was employed to reduce the temperature gradient along the capsule (less than 20 °C along the 12 mm Pt capsule). For the experiment conducted at 3.0 GPa, a 12.7 mm talc–Pyrex assembly was used. This assembly also included a tapered furnace giving a thermal gradient of less than 20 °C over a 7 mm capsule length. A pressure correction of 5% was applied for the talc Pyrex assemblies consistent with the suggested friction correction by McDade et al. (2002) for talc–Pyrex assemblies. Run durations were at least 3 h to ensure equilibrium.

Two different pressure plates were used: 1/2 inch and 3/4 inch pressure plates with a special design in which holes have been drilled to improve the experimental quench rate. The use of these two different pressure plates result in similar quench rates at the end of the experiments. The temperature quench rate for the piston cylinder apparatus was timed at more than 200 °C/s to 500 °C/s for both 3/4 and 1/2 inch pressure plates. Isobaric quenching ensured that quench (decompression) bubbles were not formed. Most of the recovered glasses are clear and crystal free; although in the samples synthesised at 2.0 and 3.0 GPa, a small fraction of corundum (on the order of a few %) was identified in the ^{27}Al NMR spectrum (see Table 1; Fig. 4C). It should be noticed that the corundum crystals were not observed optically in the glass, witnessing its very low abundance. Additionally, the recovered sample synthesised at 3.0 GPa was slightly blackened, suggesting the presence of a small proportion of graphite that might be due to a possible contact in between the Pt capsule and the graphite furnace (Brooker et al., 1998). The presence of this graphite appears not to impact the outcome of the present results.

2.2. Analytical methods

2.2.1. Electron probe micro-analyses (EPMA) for glass chemical composition

The major element compositions of glasses were measured using EPMA. Measurements were done on a Cameca SX 50, with 15 kV and 10 nA, with 10 s peak counting time for all elements. Analyses were conducted in defocused mode (10 μm beam diameter). The average major element concentrations (in wt.%) obtained from more than 20 analyses for each recovered glasses are reported in Table 1. The standard deviation for each oxide is at most 0.3 wt.% for SiO_2.

Table 1
Experimental conditions, chemical composition and CO_2 solubility in the investigated samples: basG for the high-pressure glasses and basM for molecular dynamics simulations.

	FPMD				Glass syntheses			
	basM-8-CO2	basM-8-free	basM-5-CO2	basM-5-free	basG-0.5	basG-1.5	basG-2	basG-3
Experimental conditions								
Pressure (GPa)	8.0		5.0		0.5	1.5	2.0	3.0
Temperature (K)	2073		2073		1773	1773	1798	1873
Theoretical composition and EPMA analyses in wt.%[a]								
SiO_2	48.87				47.42	47.17	n.a.	45.98
Al_2O_3	17.40				16.08	17.24	n.a.	15.49
CaO	16.33				16.92	16.00	n.a.	16.08
MgO	17.40				17.79	16.29	n.a.	16.98
Total	100				98.21	96.70	n.a.	94.53
Calculated NBO/T[b]	0.957				1.060	0.927	n.a.	1.040
Calculated NBO/Si[b]	1.358				1.483	1.326	n.a.	1.453
CO_2 solubility in wt.%[c]	19.8	0	5	0	0.37 ± 0.01	0.95 ± 0.02	1.74 ± 0.08	2.18 ± 0.22
Sample aspect					Clear glass	Clear glass	4% corundum crystals[d]	Graphite + 4% corundum crystals[d]

[a] The theoretical composition is fixed by the investigated composition in the FPMD simulations. The glass composition is determined by EPMA analyses. The error is based on replicated EPMA analyses associated with each oxide concentration. The maximum error is ±0.3 wt.% for SiO_2. Sample basG-2 was not analysed.

[b] The NBO/T and the NBO/Si are the ratio between non-bridging oxygen and the tetrahedral charges (Al^{3+} + Si^{4+} for NBO/T and Si^{4+} for NBO/Si) as calculated from the method of Mysen (1990). Both the NBO/T and NBO/Si are calculated on an anhydrous basis consistent with the experimental conditions.

[c] The wt.% CO_2 was determined using micro-Raman spectroscopy and using the method established by Morizet et al. (2013a,b). The reported error on the wt.% CO_2 is based on the replicated analyses on each sample and therefore represents the homogeneity in CO_2 solubility within the sample. Morizet et al. (2013a,b) reported a global error better than ±0.2 wt.% CO_2 at this CO_2 level.

[d] The corundum content which was not observed optically has been determined from the simulation of the ^{27}Al MAS NMR spectra (see Supplementary material).

2.2.2. Vibrational micro-raman and micro-FTIR spectroscopic measurements for volatile content determination

Confocal micro-Raman was used to quantify the dissolved CO_2 in the glass samples. The Raman system is a Jobin–Yvon Labram spectrometer (focal distance = 300 mm) equipped with a 2400 grooves/mm grating and a CCD detector. The light source is an Ar laser Innova 300-5W from Coherent© operating at 514.5 nm. The typical output laser power was set at 150 mW. The analyses were performed in confocal mode (hole = 500 μm, slit = 200 μm) with a Leitz (×40) objective. The spectra were recorded in the network and CO_3^{2-} vibrational frequency range between 200 and 1200 cm^{-1}. The spectral frequency position was measured with the emission lines of Ne- and Hg-lamps and metal-Si chip. The accuracy stays within ± 1 cm^{-1}. The acquisition time was usually within 45–90 s to obtain a reasonably good signal to noise ratio (S/N).

The glass CO_2 solubility was determined from micro-Raman spectroscopy using the calibration method of Morizet et al. (2013a,b). The method is based on a statistical analysis of the Raman stretching vibrational band of the aluminosilicate framework (800–1100 cm^{-1}) and the signature of the ν_1 CO_3^{2-} band (1070–1090 cm^{-1}). The ratio between the area of the ν_1 CO_3^{2-} and the area of the aluminosilicate stretching vibrational bands is linearly correlated to the CO_2 content. This method is applicable to glass compositions in which CO_2 is dissolved solely as CO_3^{2-} groups. This is the case in the present investigated composition and in agreement with our current knowledge of the CO_2 dissolution mechanisms (Fine and Stolper, 1986; Blank and Brooker, 1994; Dixon et al., 1995). The reader is referred to this article for further information on the method.

The wt.% CO_2 is reported in Table 1. The CO_2 solubility ranges from 0.37 to 2.18 wt.% with a typical error of less than 0.2 wt.%. This increase in CO_2 solubility is observed with increasing pressure as shown in Fig. 2 (0.37 and 2.18 wt.% CO_2 at 0.5 and 3.0 GPa, respectively) and is in good consistency with previous studies (*e.g.*Blank and Brooker, 1994; Thibault and Holloway, 1994; Brooker et al., 1999; Morizet et al., 2002; Botcharnikov et al., 2005, 2006; Behrens et al., 2009; Morizet et al., 2014a,b). The CO_2 solubility level used for FPMD simulations at 5.0 and 8.0 GPa is also reported in Fig. 2 (5.0 and 19.8 wt.% CO_2) and has been constrained from the molecular dynamics simulation results reported in Guillot and Sator (2011). The effect of temperature on CO_2 solubility is unknown because of the small number of investigated samples; however, it has been shown that at such a high temperature (1773 to 1873 K), the temperature dependency of CO_2 solubility is probably relatively reduced (Morizet et al., 2002). The range of CO_2 solubility determined for this haplo-basaltic composition is comparable to previous results on CO_2 solubility for typical basaltic compositions (Pan et al., 1991; Blank and Brooker, 1994). Moreover, the CO_2 solubility determined in the glasses is in good agreement with previous molecular dynamics calculations by Guillot and Sator (2011) for the same composition and shown in Fig. 2 for comparison. We observe a slightly lower CO_2 solubility at 3.0 GPa than suggested by Guillot and Sator (2011). This lower CO_2 solubility is likely due to the presence of graphite in this sample which induces a lower CO_2 thermodynamic activity in the fluid phase (see Morizet et al., 2010).

Although all the experiments were conducted under anhydrous conditions, micro-FTIR analysis performed on doubly polished basG-1.5

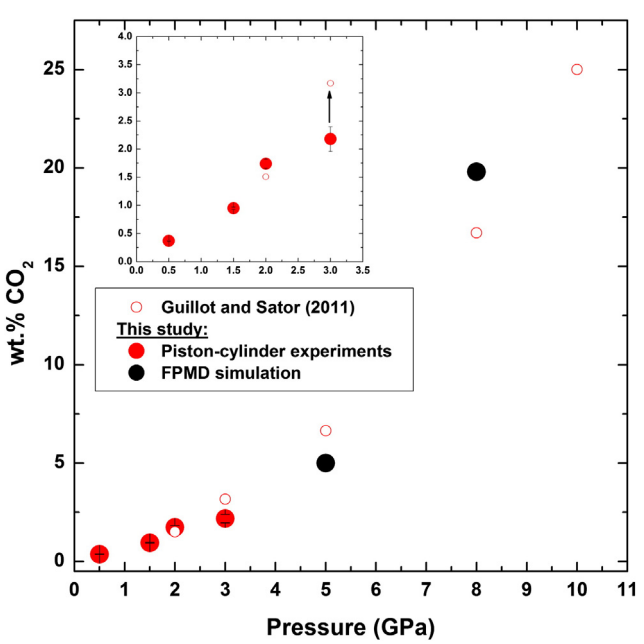

Fig. 2. CO_2 solubility in wt.% determined in the glasses quenched from piston–cylinder experiments as a function of pressure (up to 3.0 GPa) and CO_2 content used in FPMD simulations at 5.0 and 8.0 GPa. As a comparison, the CO_2 solubility data for MORB obtained by Guillot and Sator (2011) are reported. The error on the CO_2 solubility is within the points and has been determined from replicated Raman analyses using the method of Morizet et al. (2013a) in the glasses.

sample reveals the presence of a small but measurable quantity of water dissolved in the glass in the form of OH^- groups, with a band at 4500 cm^{-1}. Subsequent quantification using the Beer–Lambert approximation (Ohlhorst et al., 2001) was done considering the area of the 4500 cm^{-1} OH^- peak, the integrated extinction coefficient (230 $L \cdot mol^{-1} \cdot cm^{-2}$) proposed by Jakobsson (1997) and a density of 2950 $g \cdot L^{-1}$ as measured by the Archimedean method in toluene. Replicated measurements give a H_2O content of less than 0.3 wt.%. This amount of water could result from adsorbed water molecules onto the starting material powder prior to the experiments; alternatively, the presence of water could also be due to hydrogen diffusion through the capsule walls (Truckenbrodt and Johannes, 1999) and originate from the talc breakdown of the high pressure assembly upon heating.

2.2.3. ^{13}C, ^{27}Al and ^{29}Si solid state magic angle spinning nuclear magnetic resonance spectroscopy

Solid state ^{13}C-, ^{27}Al- and ^{29}Si-MAS NMR analyses of the partially crushed samples were performed with a 500 MHz Bruker Avance III. 4 and 2.5 mm CP/MAS probes were employed and the samples were loaded in a ZrO_2 rotor with Teflon end-cap. Rotors were spun at 10–14 kHz for ^{13}C and ^{29}Si analyses and at 30 kHz for ^{27}Al analyses. All spectra are referenced against TMS (tetramethylsilane) for ^{13}C- and ^{29}Si-MAS NMR and $Al(NO_3)_3$ in aqueous solution for ^{27}Al-MAS NMR.

^{13}C-MAS NMR spectra were acquired with single π/4 excitation of 2 μs. ^{29}Si-MAS NMR spectra were acquired with single π/2 excitation of 4 μs. For ^{13}C Direct MAS spectra, up to 1440 scans have been co-added; for ^{29}Si Direct MAS spectra, up to 280 scans have been co-added. Both ^{13}C- and ^{29}Si-species can have long spin lattice relaxation time in silicate glasses (several minutes, Kohn et al., 1991; Maekawa et al., 1991; Morizet et al., 2014a). As a result, recycle delays between scans of at least 90 s and 240 s were used for ^{13}C- and ^{29}Si-spectra accumulation, respectively. The obtained free-induction-decay signal was treated with a low line broadening exponential function (50 Hz) preventing the loss of structural information.

The 1D ^{27}Al Direct MAS NMR experiments were conducted for all the glass samples with single π/13 pulse of 3 μs with a radiofrequency field (RF) of 12 kHz. We used a recycle delay of 1 s which is standard for ^{27}Al spin relaxation in silicate glasses (Lee and Stebbins, 2000). For all the ^{27}Al Direct MAS NMR spectra, we collected 8192 scans to obtain a good S/N ratio. Additional 2D triple quantum MAS spectra (3QMAS) were also acquired using the 3-pulse sequence with Z-filtering (Amoureux et al., 1996). At RF field of 130 kHz, the 3Q excitation and reconversion pulses were set to 3.4 and 1.1 μs. The third pulse duration for signal observation was set to 6.8 μs with an RF field of 12 kHz.

Two dimensional ^{27}Al–^{29}Si J-HMQC (Heteronuclear Multiple-Quantum Correlation) and one dimensional {^{27}Al}–^{29}Si R-INEPT (Refocused INEPT, insensitive nuclei enhanced by polarisation transfer) spectra were also acquired under MAS condition (14 kHz) and using a recycle time of 1 s. The two NMR pulse sequences are given in Supplementary material. Like the widely used CP (cross-polarisation) technique, the INEPT sequence is designed to transfer nuclear magnetization between unlike spins. Nevertheless, in contrast with the through-space CP technique, INEPT is a through-bond technique making use of the scalar J coupling between unlike spins (here, a two-bonds ^{27}Al–O–^{29}Si coupling). Optimized transfer from ^{27}Al to ^{29}Si is obtained for delays within the pulse sequence which depend on the J coupling strength. For both J-HMQC and R-INEPT experiments, the ^{29}Si π/2 pulse was set to 8 μs with a RF field of 31 kHz and ^{27}Al selective π/2 pulse was set to 5.3 μs with a RF field of 10 kHz. The 2D ^{27}Al–^{29}Si J-HMQC was acquired with $\tau = 15$ ms. For the R-INEPT sequence, two delays τ and τ' are required. According to the analytical expressions of the build-up magnetization curves (Amoureux et al., 2007), the maximum signal is always observed for $\tau = 0.5/J$ where J is the ^2J(Al–O–Si) coupling value in Hz. In contrast, the optimal value for τ' depends on the multi-spin system. Clearly, in the aluminosilicate glasses, the optimal τ' is 0.167/J for Q^n(4Al), 0.196/J for Q^n(3Al) and 0.25/J for Q^n(2Al) species, whereas it is 0.5/J for Q^n(1Al) (n = 1,2,3,or 4 when possible). Therefore, performing R-INEPT experiment with $\tau = \tau'$ favours signal originated from Q^n(1Al) species. Moreover, as τ and τ' are proportional to 1/J, using smaller τ values enhances signals associated with higher J coupling values. Unfortunately, only few studies have investigated ^2J(Al–O–Si) couplings and little is known about the relationship between the J values and the local structure (Al–O–Si angle, for instance). However, all the values reported in the literature for aluminosilicates are below 30 Hz (Hiet, 2009; Florian et al., 2012). So that, the two {^{27}Al}–^{29}Si R-INEPT spectra shown in the present work were acquired with $\tau = \tau' = 15$ ms and $\tau = \tau' = 50$ ms.

2.3. First principles molecular dynamics simulation

The FPMD simulations were performed within the density functional theory (DFT) framework and the Born–Oppenheimer method using the freely available program package QUICKSTEP/CP2K (VandeVondele et al., 2005). QUICKSTEP uses a hybrid Gaussian plane-wave (GPW) method (Lippert et al., 1997). We employed a double-zeta valence plus polarisation (DZVP) basis set optimized for molecules (VandeVondele and Hutter, 2007) for all elements in the system: O, C, Si, Al, Mg and Ca. Core electrons were replaced by the Goedecker–Teter–Hutter (GTH) norm-conserving pseudo-potentials (Goedecker et al., 1996; Hartwigsen et al., 1998; Krack, 2005). The cut-off for the electronic density was set to 700 Ry and the gradient corrected exchange-correlation functional BLYP (Becke, 1988; Lee et al., 1988) was used in the DFT calculations. van der Waals interactions were taken into account using the scheme of Grimme (2006). Constant temperature conditions were imposed by a Nosé–Hoover thermostat chain (Nosé, 1984a,b). The time step for the MD simulations was 0.5 fs.

A relatively high temperature, T = 2073 K, was considered such as the viscosity of the liquid is sufficiently small, log $\eta \sim 0$ (Pa·s) at 2073 K for anhydrous natural and synthetic basaltic compositions (Giordano and Dingwell, 2003; Giordano and Russell, 2007), to allow for fast relaxation of the structures (see Section 3.2). The simulations were performed at a fixed volume. As the equation of state of the CO_2 bearing basalts is not known in the liquid state, we have estimated the density of the melt at a given pressure using the empirical force-field from Guillot and Sator (2011). Two different densities were then studied at pressures estimated to be 5 GPa (denoted basM-5-CO2) and 8 GPa (denoted basM-8-CO2) respectively according to Guillot and Sator (2011). These two systems contain 81 SiO_2, 17 Al_2O_3, 43 MgO, and 29 CaO units for the aluminosilicate part, corresponding to a haplo-basaltic composition. The amount of CO_2 corresponds to saturation as estimated by Guillot and Sator (2011); these are 56 and 12 CO_2 molecules, at 8 GPa and at 5 GPa respectively; for a total of 640 and 508 atoms. The compositions in wt.% are listed in Table 1 for comparison with the synthetic glass samples. We did not consider lower pressure, closer to the highest experimental pressure attained in the present work, because of the drop in CO_2 solubility as pressure decreases. At lower pressure and given the small system size imposed by FPMD, the number of CO_2 incorporated at saturation would be too small to be statistically meaningful. Two additional simulations were also conducted under CO_2-free conditions at 5.0 and 8.0 GPa (denoted as basM-5-free and basM-8-free in Tables 1 and 2). These two systems have the same composition as basM-8-CO2 and basM-5-CO2, except for the absence of CO_2 molecules. Both CO_2-free simulations thus contain a total of 472 atoms. In all cases, we have employed the empirical force-field from Guillot and Sator (2011) for generating the initial configurations. All simulations were then run for about 10 ps long to let the system equilibrate, followed by 10 ps long simulations used for analysis of the structures.

For these analyses, the atom connectivity was defined on an interatomic distance basis. Only bonds between oxygen and Si, Al or C were considered. An oxygen atom is said to be linked to an atom X (X = Si, Al or C), if the O–X distance is smaller than the distance of the first minimum of the O–X radial distribution. These distances are 1.8 Å for C, 2.2 Å for Si and 2.5 Å for Al.

Table 2
Speciation results from *in-situ* FPMD simulations and *ex-situ* NMR analyses: Si speciation (Q^n speciation) is reported with the calculated NBO/Si and Al speciation with the average Al coordination number. The C speciation obtained from FPMD simulations is also provided.

	FPMD[a]					Glass syntheses[b]		
	basM-8-CO2	basM-8-free	basM-5-CO2	basM-5-free	basG-0.5	basG-1.5	basG-2	basG-3
Si X Q^n speciation								
$Q^{n>4}$	0.063 (0.006)	0.081 (0.013)	0.034 (0.011)	0.042 (0.007)				
Q^4(nAl)	0.360 (0.014)	0.333 (0.020)	0.297 (0.004)	0.303 (0.016)	0.110 (0.011)	0.114 (0.011)	0.120 (0.012)	0.116 (0.012)
Q^3(mAl)	0.383 (0.015)	0.358 (0.032)	0.439 (0.018)	0.437 (0.008)	0.479 (0.048)	0.490 (0.049)	0.514 (0.051)	0.581 (0.058)
Q^2(kAl)	0.166 (0.007)	0.184 (0.004)	0.194 (0.017)	0.170 (0.017)	0.411 (0.041)	0.396 (0.040)	0.366 (0.037)	0.302 (0.030)
Q^1	0.027 (0.007)	0.034 (0.006)	0.035 (0.007)	0.047 (0.005)				
Q^0	0.000 (0.000)	0.009 (0.003)	0.001 (0.001)	0.001 (0.001)				
NBO/Si[c]	0.797 (0.041)	0.865 (0.070)	0.937 (0.077)	0.922 (0.061)	1.30 (0.130)	1.28 (0.128)	1.25 (0.125)	1.19 (0.119)
Al coordination speciation								
^{IV}Al	0.255 (0.028)	0.300 (0.036)	0.423 (0.032)	0.467 (0.037)	0.856 (0.086)	0.751 (0.075)	0.624 (0.062)	0.591 (0.059)
^{V}Al	0.514 (0.022)	0.533 (0.048)	0.469 (0.031)	0.429 (0.035)	0.129 (0.013)	0.195 (0.020)	0.280 (0.028)	0.291 (0.029)
^{VI}Al	0.227 (0.029)	0.163 (0.019)	0.104 (0.014)	0.100 (0.003)	0.015 (0.002)	0.054 (0.005)	0.055 (0.006)	0.073 (0.007)
Average Al coordination	4.96 (0.04)	4.84 (0.03)	4.66 (0.03)	4.61 (0.02)	4.16 (0.10)	4.30 (0.11)	4.41 (0.11)	4.46 (0.11)
CO_2 speciation								
CO_2^{mol}	0.123		0.184		0.000			
Free CO_3^{2-}	0.164		0.190		1.000			
NBO–carb.	0.440		0.380					
Si–carb.–Al	0.099		0.117					
Al–carb.–Al	0.136		0.050					
Si–carb.–Si	0.038		0.079					

[a] Error estimates on X Q^n speciation and Al coordination speciation from FPMD simulations are two sided confidence interval at 0.95% estimated from a Student distribution using results from five blocks of 2 ps each.
[b] The X Q^n speciation was determined from the ^{29}Si MAS NMR spectra deconvolution (see Supplementary material). We considered a typical error of 10% relative to the determined X Q^n value. This error is probably overestimated. The Al environment concentrations was determined in glasses from the ^{27}Al MAS NMR spectra simulation (see Supplementary material). We also considered a 2.5% relative error to determine the average Al coordination number within the glasses.
[c] The corresponding NBO/Si was calculated with the following equation: $\text{NBO/Si} = 4 \times \text{X } Q^0 + 3 \times \text{X } Q^1 + 2 \times \text{X } Q^2(\text{kAl}) + 1 \times \text{X } Q^3(\text{mAl})$.

3. Results

3.1. Nuclear magnetic resonance spectroscopy

3.1.1. ^{29}Si MAS NMR

A typical example of acquired ^{29}Si Direct MAS NMR spectrum is provided in Fig. 3 for basG-0.5 sample. The ^{29}Si peak is centred at −82 ppm corresponding to Si in Q^n configuration. No evidence for five coordinated Si species was identified at −150 ppm (Stebbins and Poe, 1999). The acquired ^{29}Si Direct MAS spectrum exhibits a slight peak asymmetry witnessing that the ^{29}Si spectrum is a complex convolution of individual peaks; each of these being attributed to a given Q^n species (*e.g.*Lippmaa et al., 1980; Grimmer et al., 1984; Schramm et al., 1984; Maekawa et al., 1991; Stebbins, 1995; Zhang et al., 1997; Schmidt et al., 2000; Schneider et al., 2003; Mysen and Cody, 2005; Malfait et al., 2007b; Angeli et al., 2011; Davis et al., 2011; Morizet et al., 2013b). The evidence for several Q^n species is further asserted by the various NMR experiments we have conducted. In Fig. 3A, we show a comparison between ^{29}Si Direct MAS

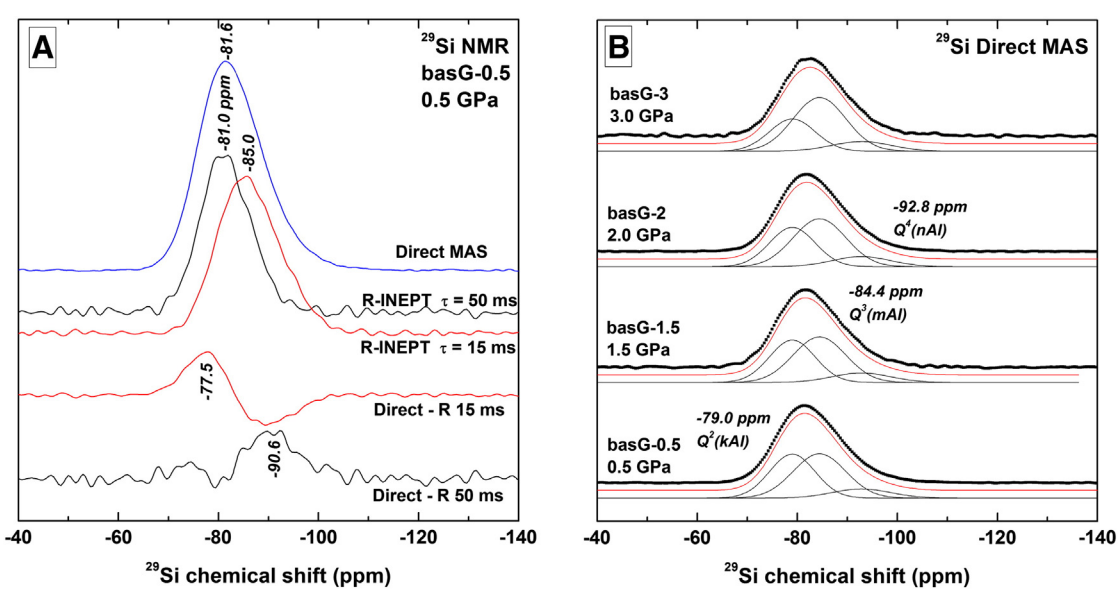

Fig. 3. A) Comparison between ^{29}Si Direct MAS NMR spectrum and ^{27}Al–^{29}Si R-INEPT NMR spectra acquired with $\tau = \tau' = 15$ and 50 ms for basG-0.5 quenched glass. The ^{29}Si Direct MAS spectrum exhibits a peak maximum at −81.6 ppm whereas the selective nature of the R-INEPT spectra (probing different Al–O–Si bonds) give peak maxima at −81.0 and −85.0 ppm. We also show the difference between the ^{29}Si Direct and R-INEPT $\tau = 15$ and 50 ms. The difference spectra suggest that the R-INEPT acquisition does not fully reproduce the ^{29}Si Direct spectrum. B) The ^{29}Si Direct MAS spectra (dotted line) were deconvoluted with three peaks (solid line). The ^{29}Si chemical shift for these peaks are −79.0, −84.4 and −92.8 ppm and each peak was assigned to Q^2(kAl), Q^3(mAl) and Q^4(nAl), respectively (see text for details on the peak assignment).

spectrum and two {^{27}Al}–^{29}Si R-INEPT spectra for basG-0.5 glass sample. We also report the difference spectra between the ^{29}Si Direct MAS and the R-INEPT NMR spectra.

As explained in the experimental section, choosing $\tau = \tau' = 1/2$ J (where J is the 2 J(Al–O–Si) coupling value) mostly favours magnetization transfer from pairs of spins (*i.e.* Q^n(1Al)). Moreover, using smaller τ values enhances signals associated with higher J coupling values. As shown in Fig. 3A, the {^{27}Al}–^{29}Si R-INEPT spectrum obtained with $\tau = \tau' = 15$ ms is centred at −85 ppm. By increasing $\tau = \tau'$ to 50 ms, the maximum of the {^{27}Al}–^{29}Si R-INEPT spectrum appears at −81 ppm (Fig. 3A). This small left-shift witnesses the existence of smaller J coupling values than those probed with $\tau = \tau' = 15$ ms. Therefore, the 4 ppm left-shift induced by increasing $\tau = \tau'$ is probably due to an increase of the Q^3(2Al) contribution to the whole signal. In contrast to the {^{27}Al}–^{29}Si R-INEPT spectrum obtained with $\tau = \tau' = 15$ ms, the one obtained with $\tau = \tau' = 50$ ms does not reproduce the lowest frequency part at −91 ppm of the ^{29}Si direct MAS spectrum as shown by the difference spectrum (Direct-R 50 ms in Fig. 3A). Since the −85 ppm was mainly associated to Q^3(1Al) species, this unobserved signal might be assigned to Q^4(pAl) species. The width of the {^{27}Al}–^{29}Si R-INEPT spectrum obtained with $\tau = \tau' = 50$ ms is also too small to reproduce the highest frequency part of the ^{29}Si direct MAS spectrum at −78 ppm. This reveals the existence of Q^n(pAl) species of lower J values such as Q^2(1Al). The presence of Q^2(0Al) and Q^3(0Al) cannot be assessed by R-INEPT experiment which is a through-bond transfer technique. However, these two species are likely to exist in our glass samples.

The ^{29}Si NMR spectrum deconvolution procedure has been reported in previous work (Morizet et al., 2013b, 2014b; and references therein). The ^{29}Si NMR spectrum deconvolution was conducted simultaneously on the entire set of spectra and using three Gaussian peaks. The simultaneity of the procedure implies that for a given Gaussian peak, the peak position and the full width at half maximum are identical from one sample spectrum to another sample spectrum and only the peak area changes. The followed approach is justified by the fact that all the glass samples have, within error, the same chemical composition as suggested by the EPMA analytical results shown in Table 1.

This procedure is an approximation since the glass structure might be described with more than three individual species. For instance, we clearly identified the presence of ^{29}Si Q^n units with various Al surrounding inducing a shift in the ^{29}Si δ_{iso} (Hiet et al., 2009); however, the impact of 5- and 6-coordinated Al unit on the ^{29}Si δ_{iso} is currently unknown. Furthermore, the fact that a given ^{29}Si Q^n species might have several Al surrounding which can be AlO_4, AlO_5 and/or AlO_6 could induce a change in the shape of the peak representing this Q^n species; hence, a Gaussian shape might not be appropriate in that case. Consequently, there is an additional complexity not taken into account in the present deconvolution procedure.

The peak assignment is reported in Table 2 along with the species abundances (X Q^n) obtained from the ^{29}Si Direct MAS simulation. The entire set of fitting parameters is provided in Supplementary material. Namely, the −79.0 ppm, −84.4 ppm and −92.8 ppm lines are assigned to Q^2(kAl), Q^3(mAl) and Q^4(nAl) species, respectively. Those derived peak positions are concomitant with the suspected components (see the comparison made between the Direct MAS and the R-INEPT spectra and the difference between both). The R-INEPT analyses clearly identified a component located at −85 ppm but two additional components were not reproduced at −77.5 and −90.6 ppm, respectively.

In the investigated basaltic glass composition, the Al/Si ratio is relatively high (0.42), and considering this value and the Al avoidance rule, it is highly possible that up to 2 Al atoms might be present in the surrounding of the Q^4(nAl) as stated by Lee and Stebbins (1999). Furthermore, a peak at around −94 ppm for Q^4(2Al) in calcium aluminosilicate glasses was reported by Lee and Stebbins (1999). In a similar way, recent work by Le Losq et al. (2014) on sodium aluminosilicate glasses, Davis et al. (2011) on magnesium silicate glasses and Zhang et al. (1997) on calcium silicate glasses reported a position for Q^3(0Al) at −91.0, −90.8 and −90.4 ppm, respectively. From a general stand point, in aluminosilicate glasses, substitution of Al for Si atom as a second neighbour in the close vicinity to a Si atom (*i.e.* substitution of Si–O–Si to Si–O–Al in tetrahedral configuration) induces a shift in ^{29}Si peak of at least +5 ppm (Engelhardt et al., 1985; Schmidt et al., 2000; Hiet et al., 2009; Le Losq et al., 2014). Therefore, a Q^3(1Al) would have a ^{29}Si δ_{iso} around −85.0 ppm. The proposed assignment to Q^3 for the identified component at −84.4 ppm (see Fig. 3B) would be in good agreement with the Q^3(1Al) species, as stated previously from R-INEPT experiments (see Fig. 3A). Furthermore, the resulting NBO/Si measured from the Q^n abundances in glasses (NBO/Si between 1.19 and 1.30, see Fig. 7, Table 2 and Eq. (4)) is totally consistent with the theoretical NBO/Si value of 1.358.

3.1.2. ^{27}Al MAS NMR

We have acquired 1D ^{27}Al Direct MAS, 2D ^{27}Al 3QMAS and ^{27}Al–^{29}Si J-HMQC NMR spectra for basG samples (Fig. 4). Multiple Al environments are identified from the ^{27}Al NMR spectra (both Direct and 3QMAS) of the quenched glasses (Fig. 4B and C). The simulations of the ^{27}Al Direct MAS NMR spectra for basG glasses were performed with DMFit software (Massiot et al., 2002) using Czsimple fitting function for ^{IV}Al, ^{V}Al and ^{VI}Al environments describing the distribution the effect of electrical field gradient (EFG) distribution on Al environments (Neuville et al., 2006). The Czsimple fitting function is derived from the Czjzek distribution function (Czjzek et al., 1981) and describes the EFG distribution around Al atoms as statistical structural disorder with a Gaussian isotropic model as a physically consistent model for disordered solids (Brand and Le Caër, 1988). Three Al environments were determined: 4-coordinated Al (AlO_4, ^{IV}Al) with $\delta_{iso} \approx +66$ ppm; 5-coordinated Al (AlO_5, ^{V}Al) with $\delta_{iso} \approx +37$ ppm; 6-coordinated Al (AlO_6, ^{VI}Al) with $\delta_{iso} \approx +6$ ppm (see Supplementary material for corresponding derived peak parameters). Those δ_{iso} peak positions are consistent with previous works (see Stebbins, 1995; Stebbins et al., 2000; Toplis et al., 2000; Neuville et al., 2006). The three Al coordination states are observed and unambiguously identified by 3QMAS ^{27}Al NMR spectra as shown in Fig. 4B for basG samples and have been observed also in basM FPMD simulations. An additional sharp signature has been also identified in basG-3 and basG-2 as shown in Fig. 4C and with a δ_{iso} ~ +16 ppm. According to Stebbins (1995), this sharp signature can be attributed to a small fraction of crystalline corundum (α-Al_2O_3).

We also show the spectrum acquired ^{27}Al-^{29}Si J-HMQC pulse sequence for basG-1.5 in Fig. 4A. This 2D spectrum confirms the interpretation proposed in Fig. 3 from ^{27}Al–^{29}Si R-INEPT spectra. We observe that ^{29}Si Q^n species (with a peak centred at −86 ppm) is correlated to all Al environments. Therefore, in addition to the Si–O–^{IV}Al bonds, both Si–O–^{V}Al and Si–O–^{VI}Al bonds also exist in the glasses. This result emphasises the importance of multiple Al environments on the global network structure of a silicate glass. Recent investigation by Le Losq et al. (2014) highlighted the important role of 5-coordinated Al in 1) the connectivity in glasses of the tetrahedral network and 2) thermodynamic properties of silicate melts.

3.1.3. ^{13}C MAS NMR

An example of typically acquired ^{13}C MAS NMR spectrum is shown in Fig. 5 for basG-1.5. The ^{13}C MAS NMR reveals that the CO_2 speciation is only represented by carbonate CO_3^{2-} species in the haplo-basaltic glasses. This speciation is consistent with previous studies on glasses of basalt-like compositions (Fine and Stolper, 1986; Pan et al., 1991; Dixon et al., 1995; Morizet et al., 2010). No CO_2^{mol} is identified contrary to what is suggested by FPMD simulations (see Table 2) and the previous work by Guillot and Sator (2011). A graphite NMR signal was observed in ^{13}C MAS NMR spectrum for basG-3. The quantity of graphite is difficult to evaluate due to the strong overlapping with the signal of the Teflon itself at +110 ppm. The graphite component appears to be

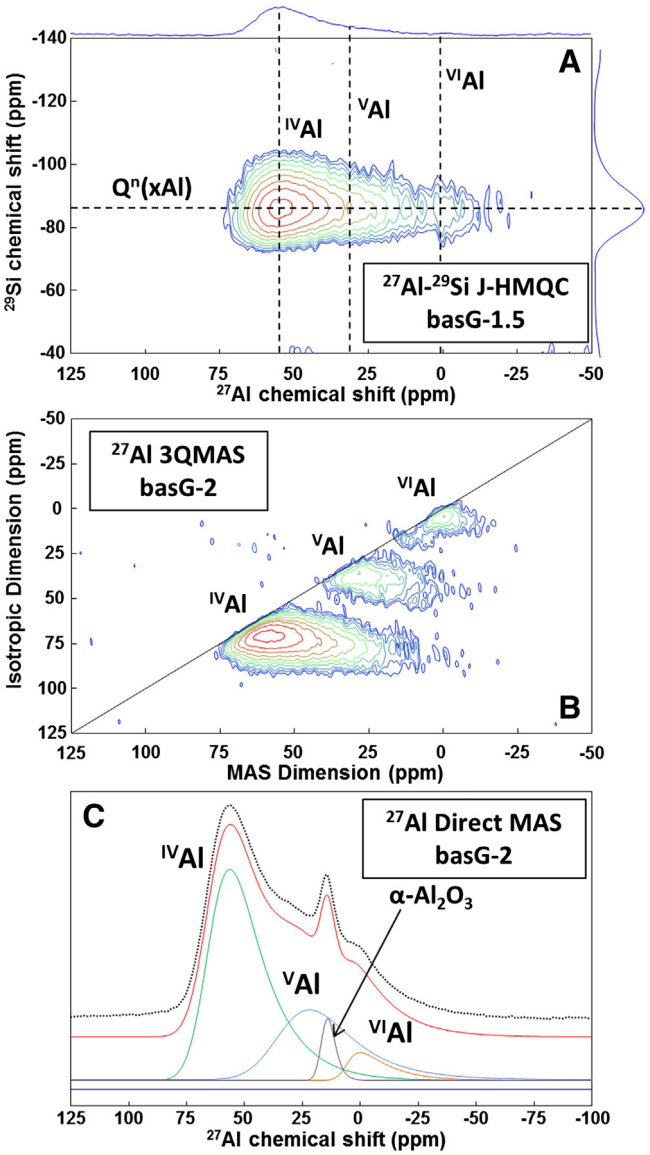

Fig. 4. A) 2D ^{27}Al–^{29}Si J-HMQC spectrum acquired with $\tau = 15$ ms on basG-1.5. The three vertical lines indicate the different Al environments. B) ^{27}Al 3QMAS NMR spectrum obtained on basG-2 showing the three distinct NMR signatures for ^{IV}Al, ^{V}Al and ^{VI}Al environments in glass (the additional signature for crystalline corundum is only weakly observable and is estimated to be roughly 4%). C) ^{27}Al Direct MAS NMR spectrum deconvolution on basG-2. The ^{27}Al spectrum is fitted with three Czsimple lines (Massiot et al., 2002) corresponding to the three Al environments; for this particular sample an additional line was placed to take into account the presence of the small fraction of crystalline corundum (α-Al_2O_3). The derived fitted parameters are available in the Supplementary material.

non-negligible; nevertheless we consider that the graphite presence does not affect dramatically the oxidized CO_3^{2-} speciation evolution in glasses. The presence of graphite implies low fO_2 conditions during the experiments. Recent work by Morizet et al. (2010) suggests that applying low fO_2 conditions induces a lowering of the CO_2 solubility as observed in Fig. 2 for this particular sample basG-3 at 3.0 GPa. However, under moderately reducing conditions, Morizet et al. (2010) did not identify a clear change in the CO_2 speciation (no presence of CH_4 for instance).

In Fig. 5, we compare ^{13}C NMR spectra collected for different CO_2-bearing glass compositions: jadeite glass (Brooker et al., 1999), haplophonolite glass (Morizet et al., 2002), nephelinite glass (Morizet et al., 2014a,b), Ca-melilitite and diopside (Morizet, unpub.). We cover a wide range of composition from fully polymerised jadeite (NBO/T = 0) to highly depolymerised diopside (NBO/T = 2) and Ca-melilitite (NBO/T = 2.6). The chemical composition is also distinct. Jadeite, phonolite and nephelinite are Na-rich composition synthesised in the Na_2O–Al_2O_3–SiO_2 and Na_2O–CaO–MgO–Al_2O_3–SiO_2 systems. Ca-melilitite, diopside and basG-1.5 are Ca–Mg-rich compositions synthesised in the Na_2O–CaO–MgO–Al_2O_3–SiO_2, CaO–MgO–SiO_2 and CaO–MgO–Al_2O_3–SiO_2 systems, respectively. This comparison will be fully discussed in Section 4.3 in order to provide constraints on the carbonate environments in the studied basaltic composition. For the basG glasses, the peak maximum is situated at +166 ppm. The width of the peak is broad and the peak is slightly asymmetric suggesting that the peak is a combination of several CO_3^{2-} environments.

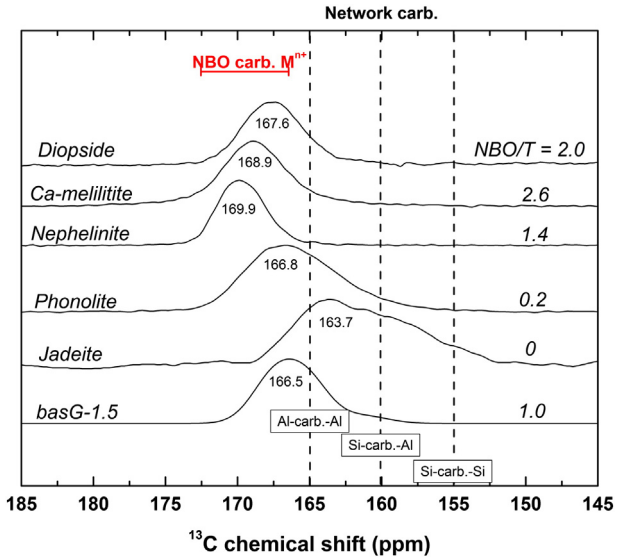

Fig. 5. Typical ^{13}C MAS NMR spectrum obtained on basG-1.5 quenched glass showing the CO_3^{2-} species. The spectrum for basG-1.5 is shown along with additional ^{13}C MAS NMR from other glass compositions with NBO/T ranging from 0 to 2.6: phonolite from Morizet et al. (2002); jadeite from Brooker et al. (1999); nephelinite from Morizet et al. (2014a,b); diopside and Ca-melilitite are unpublished data. The peak maximum is reported and ranges from + 163 to + 170 ppm. The suggested position for the different types of carbonate groups (network and NBO carb. M^{n+}) as inferred by Brooker et al. (1999, 2001) is also shown.

3.2. FPMD results

We first studied the approach towards equilibrium and the extent of the structural rearrangements with respect to the initial configuration. Fig. 6A displays the mean square displacement of the different species in basM-8-CO2 for times up to 11 ps and averaged over the first 10 ps of the simulation. The slowest species (Si) exhibits a mean square displacement of 2 Å^2 in 11 ps. The fastest species (Ca^{2+} and Mg^{2+} but also O and C) have mean square displacements around 4 Å^2. The onset of diffusion, characterized by a mean square displacement proportional to the elapsed time, is visible on Fig. 6A at the end of the time window. These mean square displacements suggest that nearest neighbour rearrangements had time to occur in the FPMD simulation such that equilibration of nearest neighbour environments has been reached. These rearrangements can have a global effect on the large scale aluminosilicate network but we cannot rule out that large scale relaxation involving long range atomic motions is insufficiently described in the FPMD simulations, retaining some memory of the initial configuration.

To further evaluate how these atomic displacements are linked to the reorganisation of the high temperature melt, Fig. 6B shows the total number of bonds in the system and the number of bonds that were conserved from the initial configuration. It can be seen that the total number of bonds reaches quickly a steady state with about 900

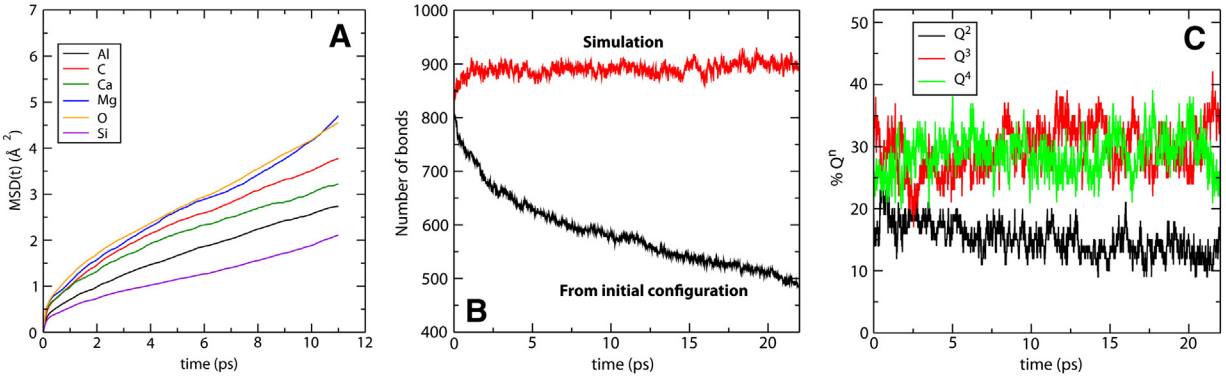

Fig. 6. A) Mean square displacement of the different species for the basM-8-CO2 simulation. The whole simulation is considered and a time average over the first 10 ps was performed. B) Total number of bonds (Si–O, Al–O and C–O) during the basM-8-CO2 simulation (red) and number of bonds conserved from the initial configuration (black). C) Evolution of the number of each Q^n species during the basM-8-CO2 simulation. (For interpretation of the references to colour in this figure legend, the reader is referred to the web version of this article.)

bonds. The number of bonds preserved from the initial condition steadily decreases as continuous reorganisation of the bonds occurs in the melt. After 10 ps, nearly 1/4 of the bonds have been broken and at the end of the simulation, only 60% of the bonds are kept intact from the initial condition. All this suggests that significant rearrangement can occur in 10 ps, which was chosen as equilibration period, and statistics will be obtained from the following 10 ps of the simulation.

Fig. 6C shows the time evolution of the population of the different Q^n species. It can be seen that during the first ps large variations occur, with inversion of the population of Q^3 and Q^4 species. These times correspond to the initial fast decay of the number of intact bonds (see Fig. 6B). Then, for times between 10 and 20 ps, used for acquiring statistics, a steady state has been reached. The basM-8-CO2 simulation corresponds to a dense melt at 8.0 GPa, therefore this gives us confidence that also at lower pressure apparent equilibrium can be reached after a few ps of equilibration at the investigated temperature (2073 K).

In Table 2, we then report the abundance of the Si Q^n species, abundance of Al coordination and speciation of carbon for all four simulations at these apparent equilibrium conditions reached in the FPMD simulations. To compute Q^n species, we have considered that a Si atom can be linked to another Si or Al either directly through an oxygen or indirectly through a bonding carbonate, since the two should have the same effect from the point of view of melt polymerisation. Very small differences, within error bars, are observed between the CO_2-free and CO_2-bearing simulations. While CO_2 molecules scavenge NBO to form carbonates, it appears that the formation of network carbonates, in particular Si–carb.–Al and Al–carb.–Al (see Table 2), compensate nearly exactly the loss of NBO oxygen ions, leaving unchanged the degree of polymerisation of the melt. Inspection of the trajectories suggests that the formation of these network carbonate species occur first *via* bonding of a CO_2 molecule to a NBO and then the formation of a new bond with a neighbouring Si or Al, and not *via* insertion of a CO_2 molecule in an already formed Si–O–Al or Al–O–Al bonds.

At this high pressure, we also observe about 6% of Si with a coordination larger than 4, namely five coordinated Si atoms. In that case, we have considered a Si atom to be Q^n if it is bound to NBO, independently of its total coordination number, extending the Q^n definition to non-purely tetrahedral Si sites as found at high temperature-high pressure. The presence of five coordinated Si is supported by recent work by Stebbins and Poe (1999) in which five coordinated Si has been identified in CaO–SiO_2 glasses quenched from 10.0 GPa. Inspection of the FPMD trajectory also indicates very mobile Q^n species. FPMD also confirms the previous assignment of NMR spectra with only a minority of Si atoms found to form Q^3(0Al) or Q^4(0Al) species, with abundances of 10% and 5% in relative to the total Q^3 and Q^4 species, respectively.

For Al coordination, we similarly observe a very small effect of CO_2 dissolution. However, both Q^n species and Al coordination show an increase of polymerisation with pressure. Q^4, Al^V and Al^{VI} species follow the evolution of pressure, while Q^3 and Al^{IV} species evolve the opposite way.

The most important difference observed between NMR analyses of the glasses and the FPMD simulation is the existence of additional species identified in the FPMD results. For instance, the FPMD simulation shows that CO_2 is also present in the high temperature melt as Free clusters of CO_3^{2-} and CO_2^{mol} species. The abundances of those species cannot be neglected (more than 15%). The significance of such a difference in CO_2 speciation between NMR on glasses and FPMD simulation on melt will be addressed further in Section 4. At first, it seems to confirm that CO_2 speciation cannot be approached adequately in *ex-situ* glasses and that CO_2 speciation in the haplo-basaltic glass is different from the CO_2 speciation in the melt under high temperature conditions.

4. Discussion

4.1. Aluminosilicate framework speciation determined from spectroscopy and FPMD

4.1.1. Q^n species distribution and NBO/Si

The peak areas derived from the ^{29}Si NMR spectrum deconvolution in Fig. 3 are directly proportional to the abundance, X Q^n, of the species (expressed as a molar fraction). The X $Q^n$is given in Table 2 and is represented in Fig. 7A. The error considered for each X Q^n is 10% relative to the value. This error is on the order of what is commonly assumed (a few % error on the X Q^n is considered in Malfait et al., 2007a,b). With increasing pressure, there is a clear decrease in X Q^2 between 0.41 at 0.5 GPa to 0.30 at 3.0 GPa in the glasses. We observe an opposite trend for X Q^3(mAl) which varies from 0.48 at 0.5 GPa to 0.58 at 3.0 GPa in the glasses. The concentration in Q^4(nAl) in the glasses is constant (X Q^4(nAl) ~ 0.11) with increasing pressure from 0.5 to 3.0 GPa.

The comparison in between the Q^n distribution observed in glass and in high temperature melt from Fig. 7A reveals that the distribution of Q^n species in glass and high temperature melt cannot be reconstructed adequately. The major difference between melt and glass is observed for Q^4(nAl). A large jump in X Q^4(nAl) is seen from 3.0 to 5.0 GPa with X Q^4(nAl) changing from 0.11 measured in glass to 0.30 determined in melt. The difference between melt and glass is less important for Q^3(mAl) but the tendency observed in glass is inverse to the one observed in melt. On the contrary, the evolution of X Q^2 in glass and melt seems in good agreement: increasing pressure induces a decrease in X Q^2. This suggests that upon increasing pressure, the proportion of X Q^3(mAl) first increases but then decreases upon further pressure increase and upon going from the glass to the high temperature melt as a result of some X Q^3(mAl) species being converted in X Q^4(nAl).

The X Q^n results obtained from the FPMD under CO_2-free conditions are also reported in Table 2 and in Fig. 7A (*open symbol*, for clarity the error on these points is not shown but provided in Table 2). The absence

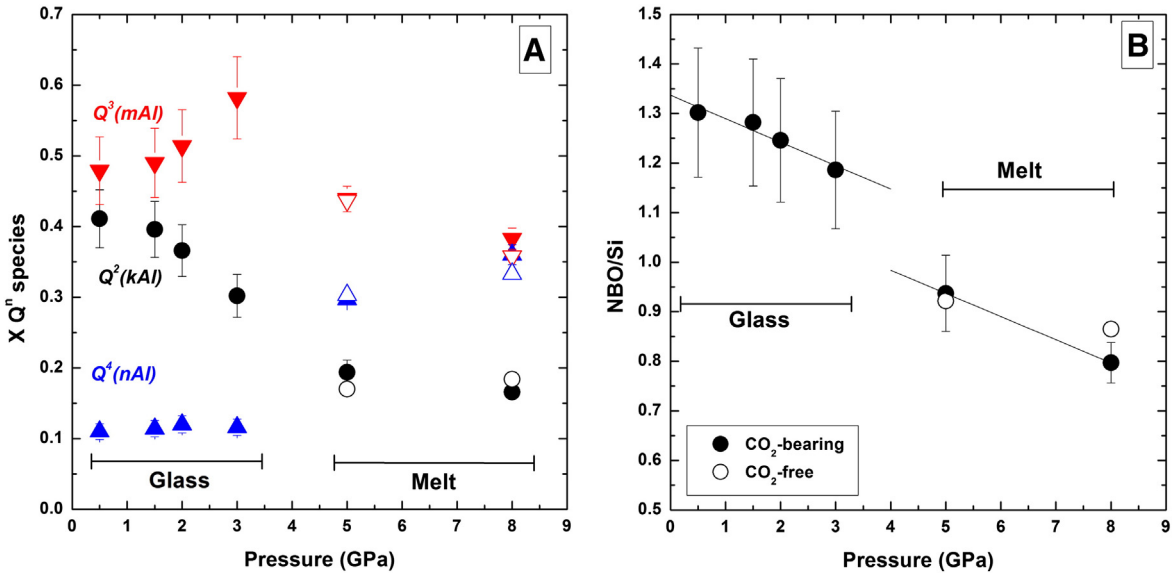

Fig. 7. A) X Q^n evolution as a function of pressure and determined for 1) the *ex-situ* glass and 2) the *in-situ* high temperature melt FPMD simulations. The open symbols correspond to the FPMD results obtained for CO_2-free conditions (basM-free in Table 2). A typical error of 10% relative to the X Q^n value was applied on the derived X Q^n from glasses analyses and is far above the possible analytical error or simulation error. For clarity, we did not add the error bars for basM-free X Q^n values. B) From the determined X Q^n, the NBO/Si is calculated and reported as a function of pressure. Hypothetical linear trends are added for the evolution of the NBO/Si for the glass and the melt. Those linear trends are extrapolated to 4.0 GPa in order to compare the apparent degree of polymerisation in both the glass and the melt.

of CO_2 does not seem to influence the abundances of the Q^n species. For instance, at 8.0 GPa for basM-8-CO2 (with ~20 wt.% CO_2) and basM-8-free, the X Q^n changes do not exceed 10% in relative to the value: X Q^4(nAl) 0.36 to 0.33; X Q^3(mAl) 0.38 to 0.36; X Q^2 0.17 to 0.18 for basM-8-CO2 and basM-8-free, respectively. The same applies to the results obtained at 5.0 GPa: the distribution of Q^n species is almost identical in between CO_2-free and CO_2-bearing (with 5 wt.% CO_2) conditions. In the light of these result, it appears that CO_2 might have a limited impact on the degree of melt polymerisation. Seifert et al. (2013) ended up to the same suggestion. Based on acoustic measurements, Seifert et al. (2013) showed that the structure of the CO_2-bearing glass seems weakly affected by the presence of CO_2 dissolved in the silicate glass network.

Using the X Q^n values, we calculated the resulting NBO/Si representative of the degree of polymerisation using the following equation (Eq. (4)) proposed in earlier studies (*e.g.*Frantz and Mysen, 1995):

$$\mathrm{NBO/Si} = 1 \times XQ^3 + 2 \times XQ^2 + 3 \times XQ^1 + 4 \times XQ^0. \quad (4)$$

The calculated NBO/Si does not represent the actual true NBO/T. The true NBO/T can only be approximated owing to the fact that the exact configuration of Al species is unknown. For instance, under hydrated conditions, it is currently assumed that four coordinated Al can adopt q^4 and q^3 configurations (Zeng et al., 1999, 2000; q^n species for Al atoms are indicated with lower case in order to avoid confusion with the Q^n species for Si atoms). Moreover, the presence of Al in higher coordination (^{V}Al and ^{IV}Al, see Fig. 4), for which the impact on the degree of polymerisation is still poorly constrained (Le Losq et al., 2014), prevents from estimating a true value for the NBO/T. As a result, the use of NBO/Si instead of the NBO/T is preferred.

For FPMD simulations, the NBO/Si was calculated without considering the Si–O–CO_2 linkages observed. In other words, a Q^2 species connected to a CO_2 molecule to form a CO_3^{2-} group through NBO consumption (*e.g.* NBO–carb. unit, see Section 3.1.3) is still considered as a Q^2 species and not as a Q^3 species. This is consistent with the fact that CO_2 is not considered as a network former.

The resulting NBO/Si values are reported in Fig. 7B for glasses and high temperature melts. The average NBO/Si measured in glasses is on the order of 1.25 which is in total consistency with the theoretical value for the NBO/Si of 1.358 (see Table 1) and also confirms the proposed assignment in Fig. 3B. We observe a clear decrease in the NBO/Si with increasing pressure: from 1.30 at 0.5 GPa to 1.19 at 3.0 GPa and down to 0.80 at 8.0 GPa (basM-8-CO2-2). The NBO/Si trend reported in Fig. 7B also suggests that the degree of polymerisation is slightly different in between the melt and the glass for the studied composition.

At both 8.0 and 5.0 GPa, the determined NBO/Si is almost identical in between CO_2-free and CO_2-bearing (5 wt.% CO_2) simulation conditions. Therefore, the change in high temperature melt polymerisation upon CO_2 addition appears undetectable for such a melt composition. This result contrasts with recent works (Mysen, 2012, 2013) which suggested a net polymerisation effect for CO_2 molecules dissolved as CO_3^{2-} groups. We suggest that if this effect exists it is relatively reduced though.

4.1.2. Al species and average Al coordination number

Al environments abundances are compiled in Table 2 and are shown in Fig. 8 as a function of experimental pressure. We observe in Fig. 8A that increasing pressure induces an increase in the coordination degree of the Al atoms: 4-coordinated Al atoms decrease, 5- and 6-coordinated Al atoms increase. Those trends in the Al coordination are pursued in the high temperature melt state as seen from FPMD simulation results. Interestingly, the abundance of each Al species is comparable in between the glass and the high temperature melt. As for X Q^n, the impact of CO_2 on the Al speciation is limited. At 5.0 and 8.0 GPa, the abundances of Al species are almost identical in between CO_2-free and CO_2-bearing FPMD simulation conditions (see Table 2).

Using the Al environment concentrations obtained by NMR deconvoluted spectra and FPMD simulations, we calculated the average coordination number of Al atoms for the studied composition. The results are shown in Fig. 8B as a function of experimental pressure. Between 0.5 and 3.0 GPa, there is a gradual increase in Al coordination from 4.16 to 4.46. This increase is also suggested by the results obtained from FPMD simulations with an average Al coordination increasing from 4.6 to 4.9 at 5.0 and 8.0 GPa, respectively. This clear increase of Al coordination both in glass and high temperature melt with increasing pressure is currently well-accepted (Allwardt et al., 2005, 2007; Lee, 2010, 2011; Lee et al., 2012). As suspected, 1) the average Al coordination number is comparable in *ex-situ* glass and *in-situ* melt and 2) the impact of CO_2 on the average Al coordination number is weak.

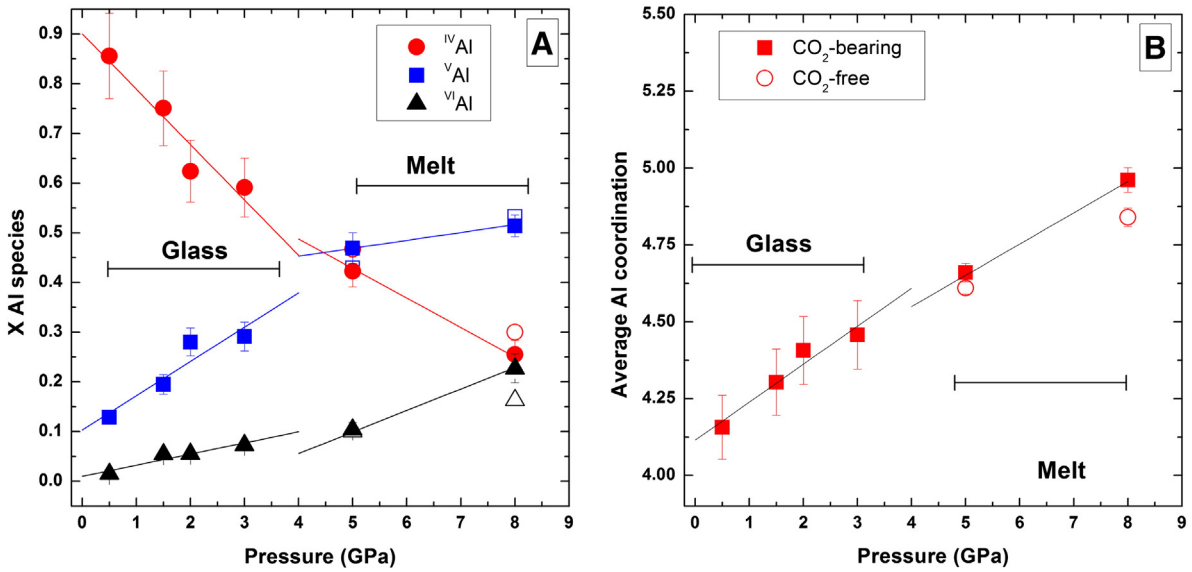

Fig. 8. A) Evolution of the Al species (^{IV}Al, ^{V}Al and ^{VI}Al) as determined in the glass and the melt from ^{27}Al Direct MAS NMR spectra deconvolution and the FPMD simulations, respectively. B) The average Al coordination number calculated from the species abundances (see Table 2). The average Al coordination number is also reported for the simulation under CO_2-free conditions (basM-free). Hypothetical linear trends are added for the evolution of the average Al coordination number for the Glass and the Melt. Those linear trends are extrapolated to 4.0 GPa so as to compare the average Al coordination number in both the glass and the melt.

4.2. Comparison between in-situ melt and ex-situ glass

For CO_2-bearing conditions, it was impossible to compare molecular structure at identical intensive conditions (P and T) for glass and high temperature melt; however, we investigate close P conditions with *ex-situ* and *in-situ* conditions: up to 3.0 GPa for glass and down to 5.0 GPa for melt. Because, we observe well constrained trends for NBO/Si (Fig. 7B) and average Al coordination number (Fig. 8B), we attempted a linear extrapolation for those parameters for glass and melt up and down to 4.0 GPa, respectively. Those extrapolations are represented by the linear trend in Figs. 7B and 8B.

At 4.0 GPa, the change in the NBO/Si between glass and high temperature melt is 0.15 in NBO/Si unit with a change from 1.15 in glass to 1.00 in melt. This change is on the order of 10% towards a decrease in the degree of polymerisation from *in-situ* to *ex-situ*. The change in the average Al coordination between glass and melt at 4.0 GPa is even lower and on the order of 1% change in relative to the value: 0.06 unit between melt (4.55) and glass (4.61).

It should be emphasised that such results can only be applicable to the currently studied composition and might not be extended to other compositions. Nevertheless, it appears possible to extract from the glass, which recorded the aluminosilicate network structure of the melt at Tg, the degree of polymerisation and the average Al coordination prevailing in the high temperature melt by applying a slight correction. In other words, the aluminosilicate network molecular structure in the high temperature melt can be straightforwardly approximated through the determination of the aluminosilicate network molecular structure in the glass which recorded the aluminosilicate network molecular structure of the melt at the glass transition temperature. This result is consistent with the recent work by Malfait et al. (2014) who demonstrated that the structure densification of the melt is preserved in the glass upon quenching. Malfait et al. (2014) showed that this observation holds true for pressure up to 3.5 GPa. In the present work, we might extend this observation to higher pressure and to CO_2-bearing aluminosilicate glasses and melts. Furthermore, Sanloup et al. (2013) have shown that the Si coordination in glass and melt is similar in both glass and melt at pressure up 35 GPa.

Although those recent studies (Sanloup et al., 2013; Malfait et al., 2014) comfort our conclusions suggesting that the aluminosilicate network structure recorded in the glass is close to the aluminosilicate network structure recorded in the melt, it is commonly assumed that the molecular structure in the high temperature melt is different from the molecular structure of the equivalent glass owing to the increase in structural disorder with increasing temperature (Dubinsky and Stebbins, 2006). Several hypotheses can be formulated to explain the aluminosilicate network of the glass being very close to its high temperature counterpart. The first hypothesis is that the glass transition temperature is higher than expected and the frozen-in molecular structure is representing a molecular structure close to the high temperature melt one. This hypothesis is unlikely considering that the effective quench rate in piston–cylinder experiments is slow. The second hypothesis is that our FPMD simulations were not fully equilibrated and the apparent equilibrium aluminosilicate network molecular structure recorded in the high temperature melt is biased by the empirical potential used to generate the initial configurations. A third hypothesis, which would need to be verified, is that the presence of CO_2 dissolved as CO_3^{2-} groups prevents the rearrangements of the aluminosilicate network molecular structure during the glass transition. In other words, the CO_3^{2-} group dissolution preserves a high aluminosilicate network structural disorder.

The lower NBO/Si in the melt as compared to the NBO/Si in the glass is directly linked to the strong change of X Q^n observed between the glass and the high temperature melt. A simple linear extrapolation of the NBO/Si trend in the glass would reach NBO/Si = 1 at a pressure of 7.0 GPa, whereas extrapolation from the high temperature melt values reaches NBO/Si = 1 at 4.0 GPa.

There can then be two origins for the lowering of the NBO/Si ratio. First, NBO oxygen could be consumed by the addition of CO_2 molecules, which would be incorporated following the evolution of pressure, because of the higher solubility of CO_2 at higher pressure. However, an identical result is found for the CO_2 free simulation suggesting that this is not the origin of the low NBO/Si ratio. Second, the total number of bonds involving network-forming atoms increases with increasing intensive conditions. This is clearly supported by the increase of Al coordination both observed experimentally and found in the simulations. The trend obtained from NMR and FPMD is here very much consistent. Hence the increase in the Al coordination is accompanied by an overall decrease of NBO/Si with pressure. However, those changes do not explain the contrasted behaviour observed in the glass and in the high temperature melt.

However, simulation predicts in the melt the presence of higher coordination of Si with Q^5 species having an abundance of about 6%. If upon cooling, these spurious configurations are eliminated at the glass transition temperature such that only tetrahedral Si is found in the glass as expected, this would lead to an increase in the number of NBO by about that same amount, 6% of the Si, within error bars of the observed 15% jump between the glass and melt NBO/Si ratios.

4.3. Carbon dioxide speciation in melt and glass

The first striking observation on carbon dioxide speciation is that the results in the glass and in the high temperature melts show a lack of consistency. Whereas CO_2^{mol} is absent from the analysed glasses (CO_2 is only present as CO_3^{2-} units), the FPMD simulations obtained at 5.0 and 8.0 GPa clearly identify the presence of CO_2^{mol} (>12%) in the melt at 2073 K.

On the contrary, we observe a good agreement in between the ^{13}C NMR results and the FPMD simulation results for the identified carbonate units. In Fig. 5, we compare ^{13}C NMR spectra obtained on various glass compositions. In their study, Brooker et al. (1999) identified three different types of carbonates in fully polymerised glass compositions such as jadeite: Al–carb.–Al, Si–carb.–Al and Si–carb.–Si located at +165, +160 and +155 ppm, respectively. Those units are network carbonates in a sense that a CO_3 molecule is linked to one tetrahedra on each side (see Kohn et al., 1991 for details). The network carbonates are present in fully polymerised (jadeite) and slightly depolymerized (phonolite) compositions (Morizet et al., 2002). Additional ^{13}C NMR signatures are observed at higher chemical shift and are attributed to NBO–carb. M^{n+} units. Those NMR signatures have been reported in previous studies (Brooker et al., 1999; Morizet et al., 2002, 2010) and are often identified in depolymerized compositions as seen in Fig. 5. The nature of the surrounding cation in the NBO–carb. M^{n+} units is yet to be clarified; however, inFig. 5, we can see that inNa-rich compositions nephelinite exhibits a peak maximum close to +170 ppm whereas Ca- and Mg-rich Ca-melilitite and diopside have a peak maximum between +168 and +169 ppm. Therefore, one can postulate that higher ^{13}C chemical shift (≥+170 ppm) would correspond to NBO–carb. with Na^+ environments; whereas lower ^{13}C chemical shift (+168–169 ppm) would correspond to NBO–carb. with Ca^{2+} and/or Mg^{2+} environments.

In Fig. 5, the peak maximum for basG-1.5 glass is situated at the frontier between the network and the NBO carbonate regions at +166 ppm. The tail in the spectrum extends down to +160 ppm suggesting that network carbonates are present in the glass. The nature of the network carbonate is unknown without relevant spectrum deconvolution; however, following the work of Brooker et al. (1999), Al–carb.–Al and Si–carb.-Al might be present in this basaltic glass composition. Additional NBO–carb. M^{n+} units are also suspected as the carbonate peak extends up to +172 ppm. Because the investigated composition is synthesised in the $CaO–MgO–Al_2O_3–SiO_2$ system, we strongly suggest that NBO–carb. Ca^{2+} or NBO–carb. $Mg^{2+}$is present in the glass. It would also be in agreement with the ^{13}C NMR signature for CO_2-bearing diopside glass shown in Fig. 5. The presence of both network and NBO carbonates units is corroborated by the results obtained with FPMD simulations (see Table 2) which identify Si–carb.–Al and Al–carb.–Al as network carbonates (on the order of 25% at 8.0 GPa) and NBO carbonate units (on the order of 40% at 8.0 GPa).

Although there is a qualitative agreement in terms of CO_3^{2-} suggestion in between glass and high temperature melt, the presence of CO_2^{mol} as identified by FPMD simulations suggests that both CO_2-bearing melt and CO_2-bearing glass may not be adequately compared for CO_2 speciation.

However, FPMD simulations taken as representative of the *in-situ* high temperature conditions suffer from possible defects. First, we should bear in mind that it relies on density functional theory; and second, the unavoidable small size and short time-scale of the FPMD simulation may constitute a major limitation. If it appears clear that the CO_2 speciation measured in glasses does not provide a true picture of the CO_2 speciation in the high temperature melt, it is yet not sure that our apparent equilibrium FPMD results can yet be considered as fully representative of the melt under high temperature *in-situ* conditions. However, while the limited time-scale in the FPMD simulations makes hard to evaluate the amount of CO_2^{mol}, FPMD simulations also point out with better confidence towards a significant amount of free CO_3^{2-} clusters with charge compensating cations (15% at 8.0 GPa). It is also possible that the solubility of CO_2 is not well evaluated from empirical force-field simulations and that the systems investigated here are oversaturated in CO_2, which is expected to promote the CO_2^{mol} species since the structure is not able to accommodate for the extra CO_2. It should finally be noted, that this difference between glass and melt could well be connected with the difference in Q^n speciation, in particular with the presence of five coordinated Si found in the melt simulation. By consuming NBO atoms, these species could make the system more favourable to CO_2^{mol}. Therefore, more solid evidences are required to fully constrain the CO_2 speciation in the melt under high temperature conditions in particular for basaltic glasses.

5. Future work and concluding remarks

The presented work aimed at comparing the molecular structure in recovered silicate glasses, representing the molecular structure of the melts frozen-in at the glass transition temperature, and the molecular structure determined from first-principles molecular dynamics simulations of melts at high pressure and high temperature conditions. We focussed our efforts on CO_2-bearing simple haplo-basaltic composition. Several samples were synthesised at high pressure and the recovered glasses were investigated *via* spectroscopic method. Molecular dynamics simulations were conducted at higher pressure on the same composition so as to investigate the aluminosilicate network molecular structure in presence of CO_2.The main conclusion is that the comparison between the aluminosilicate network molecular structure of the glass and the molecular structure of the high temperature melt from FPMD simulations is possible. In detail, we show that:

- The average Al coordination number determined in the glasses is totally consistent with the average Al coordination observed by FPMD simulations for the high temperature melts: Increasing the pressure induces an increase in the average Al coordination as expected both in the glass and in the high-temperature melt.
- The degree of polymerisation (expressed as the NBO/Si) is compared adequately using both methods. The NBO/Si increases with increasing pressure in agreement with previous works. Although, a complex structural mechanism has to be invoked so as to explain the change in the Si Q^n abundances in between the low pressure (P < 3.0 GPa) glass structure preserved at Tg and the high pressure (5.0 and 8.0 GPa) melt structure held at 2073 K.
- The configuration of the CO_3^{2-} environments as suggested by FPMD simulations is also comparable to the CO_3^{2-} environments observed in glasses: Both network and non-bridging CO_3^{2-} environments are present in the investigated simplified basaltic composition.

There is a discrepancy concerning CO_2 speciation. Whereas FPMD simulations do not rule out the existence of CO_2^{mol} species in the haplo-basaltic melt at high temperature, analysed glasses do not show any evidence of such unit. The difference in CO_2 speciation between melt and glass was put forward for different composition but has never been documented for basaltic composition. Further experimental investigations are required so as to provide observable proofs of the complex behaviour of the CO_2 speciation. For instance, *in-situ* experiments in diamond anvil cell would be extremely useful in deciphering

the CO_2 speciation under high temperature melt conditions for basalt-like compositions.

Acknowledgement

This work was performed using HPC resources from GENCI-CINES/IDRIS (Grants x2013086383 and x2014082309). Special thanks to Ida Di Carlo for helping with the EPMA analyses. The authors are grateful to the ANR agency which financed the current work through the ANR-2010-BLAN-621 "Electrolith". The authors thank the University of Orléans, the University of Nantes and the CNRS for their access to analytical facilities.

Appendix A. Supplementary data

Supplementary data to this article can be found online at http://dx.doi.org/10.1016/j.chemgeo.2015.03.021.

References

Allwardt, J.R., Stebbins, J.F., Schmidt, B.C., Frost, D.J., Withers, A.C., Hirschmann, M.M., 2005. Al coordination and density of high-pressure aluminosilicate glasses. Am. Mineral. 90, 1218–1222.

Allwardt, J.R., Stebbins, J.F., Terasaki, H., Du, L.-S., Frost, D.J., Withers, A.C., Hirschmann, M.M., Suzuki, A., Ohtani, E., 2007. Effect of structural transitions on properties of high-pressure silicate melts: ^{27}Al NMR, glass densities, and melt viscosities. Am. Mineral. 92, 1093–1104.

Amoureux, J.-P., Fernandez, C., Steuernagel, S., 1996. Z filtering in MQMAS NMR. J. Magn. Reson. Ser. A 123, 116–118.

Amoureux, J.-P., Trebosc, J., Wiench, J., Pruski, M., 2007. HMQC and refocused-INEPT experiments involving half-integer quadrupolar nuclei in solids. J. Magn. Reson. 184, 1–14.

Andersen, T., Neumann, E.-R., 2001. Fluid inclusions in mantle xenoliths. Lithos 55, 301–320.

Angeli, F., Villain, O., Schuller, S., Ispas, S., Charpentier, T., 2011. Insight into sodium silicate glass structural organization by multinuclear NMR combined with first-principles calculations. Geochim. Cosmochim. Acta 75, 2453–2469.

Becke, A., 1988. Density-functional exchange-energy approximation with correct asymptotic behavior. Phys. Rev. A 38, 3098–3100.

Behrens, H., Misiti, V., Freda, C., Vetere, F., Botcharnikov, R.E., Scarlato, P., 2009. Solubility of H_2O and CO_2 in ultrapotassic melts at 1200 and 1250 °C and pressure from 50 to 500 MPa. Am. Mineral. 94, 105–120.

Belonoshko, A.B., 1994. Molecular dynamics of $MgSiO_3$ perovskite at high pressures: equation of state, structure and melting transition. Geochim. Cosmochim. Acta 58, 4039–4047.

Belonoshko, A.B., Dubrovinsky, L.S., 1996. Molecular dynamics of NaCl (B1 and B2) and MgO (B1) melting: two-phase simulation. Am. Mineral. 81, 303–316.

Blank, J.G., Brooker, R.A., 1994. Experimental studies of carbon dioxide in silicate melts: solubility, speciation and stable carbon isotope behaviour. In: Carroll, M.R., Holloway, J.R. (Eds.), Volatiles in Magmas (Reviews in Mineralogy) 30. Mineral. Soc. Am., Washington, DC, pp. 157–186.

Botcharnikov, R.E., Freise, M., Holtz, F., Behrens, H., 2005. Solubility of C–O–H mixtures in natural melts: new experimental data and application range of recent models. Ann. Geophys. 48, 634–646.

Botcharnikov, R.E., Behrens, H., Holtz, F., 2006. Solubility and speciation of C–O–H fluids in andesitic melt at T = 1100–1300 °C and P = 200 and 500 MPa. Chem. Geol. 229, 125–143.

Brand, R.A., Le Caër, G., 1988. Improving the validity of Mössbauer hyperfine parameter distributions: the maximum entropy formalism and its applications. Phys. Res. B 34, 272–284.

Brandiss, M.E., Stebbins, J.F., 1988. Effects of T on the structures of silicate liquids: ^{29}Si NMR results. Geochim. Cosmochim. Acta 52, 2659–2669.

Brey, G.P., Green, D.H., 1975. The role of CO_2 in the genesis of olivine melilitites. Contrib. Mineral. Petrol. 49, 93–103.

Brey, G.P., Green, D.H., 1976. Solubility of CO_2 in olivine melilitite at high pressures and role of CO_2 in the Earth's upper mantle. Contrib. Mineral. Petrol. 55, 217–230.

Brooker, R.A., Holloway, J.R., Hervig, R., 1998. Reduction in piston–cylinder experiments: the detection of carbon infiltration into platinum capsules. Am. Mineral. 83, 985–994.

Brooker, R.A., Kohn, S.C., Holloway, J.R., McMillan, P.F., Carroll, M.R., 1999. Solubility, speciation and dissolution mechanisms for CO_2 in melts on the $NaAlO_2$–SiO_2 join. Geochim. Cosmochim. Acta 63, 3549–3565.

Brooker, R.A., Kohn, S.C., Holloway, J.R., McMillan, P.F., 2001. Structural controls on the solubility of CO_2 in silicate melts. Part II: IR characteristics of carbonate groups in silicate glasses. Chem. Geol. 174, 241–254.

Car, R., Parrinello, M., 1985. Unified approach for molecular dynamics and density-functional theory. Phys. Rev. Lett. 55, 2471.

Czjzek, G., Fink, J., Gotz, F., Schmidt, H., Coey, J.M.D., Rebouillat, J.P., Lienard, A., 1981. Atomic coordination and the distribution of electric-field gradients in amorphous solids. Phys. Rev. B Condens. Matter 23, 2513–2530.

Davis, M.C., Sanders, K.J., Grandinetti, P.J., Gaudio, S.J., Sen, S., 2011. Structural investigations of magnesium silicate glasses by ^{29}Si 2D Magic-Angle Flipping NMR. J. Non-Cryst. Solids 357, 2787–2795.

Dingwell, D.B., 1995. Relaxation in silicate melts: some applications. In: Stebbins, J.F., McMillan, P.F., Dingwell, D.B. (Eds.), Structure, Dynamics and Properties of Silicate Melts (Reviews in Mineralogy) 32. Mineral. Soc. Am., Washington, DC, pp. 21–66.

Dixon, J.E., 1997. Degassing of alkalic basalts. Am. Mineral. 82, 368–378.

Dixon, J.E., Stolper, E.M., Holloway, J.R., 1995. An experimental study of water and carbon dioxide solubilities in mid-ocean ridge basaltic liquids. Part I: calibration and solubility models. J. Petrol. 36, 1607–1631.

Draper, D.S., Green, D.H., 1997. P–T phase relations of silicic alkaline, aluminous mantle xenolith glasses under anhydrous and C–O–H fluid saturated conditions. J. Petrol. 38, 1187–1224.

Dubinsky, E.V., Stebbins, J.F., 2006. Quench rate and temperature effects on framework ordering in aluminosilicate melts. Am. Mineral. 91, 753–761.

Eggler, D.H., 1974. Effect of CO_2 on the melting of peridotite. Carnegie Institute Washington Yearbook 73, 215–224.

Engelhardt, G., Nofz, M., Forkel, K., Wihsmann, F.G., Magi, M., Samoson, A., Lippmaa, E., 1985. Structural studies of calcium aluminosilicate glasses by high-resolution solid-state ^{29}Si and ^{27}Al magic angle spinning nuclear magnetic resonance. Phys. Chem. Glasses 26, 157–165.

Falloon, T.J., Green, D.H., 1989. The solidus of carbonated, fertile peridotite. Earth Planet. Sci. Lett. 94, 364–370.

Fine, G., Stolper, E.M., 1986. Dissolved carbon dioxide in basaltic glasses: concentrations and speciation. Earth Planet. Sci. Lett. 76, 263–278.

Florian, P., Veron, E., Green, T.F.G., Yates, J.R., Massiot, D., 2012. Elucidation of the Al/Si ordering in gehlenite $Ca_2Al_2SiO_7$ by combined ^{29}Si and ^{27}Al NMR spectroscopy/quantum chemical calculations. Chem. Mater. 24, 4068–4079.

Frantz, J.D., Mysen, B.O., 1995. Raman spectra and structure of BaO–SiO_2, SrO–SiO_2 and CaO–SiO_2 melts to 1600 °C. Chem. Geol. 121, 155–176.

Gerlach, T.M., Graeber, E.J., 1985. Volatile budget of Kilauea volcano. Nature 313, 273–277.

Giggenbach, W.F., 1997. Relative importance of thermodynamic and kinetic processes in governing the chemical and isotopic composition of carbon gases in high-heat flow sedimentary basins. Geochim. Cosmochim. Acta 61, 3763–3785.

Giordano, D., Dingwell, D.B., 2003. Viscosity of hydrous Etna basalt: implications for Plinian-style basaltic eruptions. Bull. Volcanol. 65, 8–14.

Giordano, D., Russell, J.K., 2007. A rheological model for glassforming silicate melts in the systems CAS, MAS, MCAS. J. Phys. Condens. Matter 19, 205148.

Goedecker, S., Teter, M., Hutter, J., 1996. Separable dual-space Gaussian pseudopotentials. Phys. Rev. B 54, 1703–1710.

Grimme, S., 2006. Semiempirical GGA-type density functional constructed with a long-range dispersion correction. J. Comput. Chem. 27, 1787.

Grimmer, A.R., Magi, M., Hähnert, M., Stade, H., Samoson, A., Wieker, W., Lippmaa, E., 1984. High resolution solid state ^{29}Si NMR spectroscopic studies of binary alkali silicate glasses. Phys. Chem. Glasses 25 (4), 105–109.

Guillot, B., Sator, N., 2007a. A computer simulation study of natural silicate melts. Part I: low pressure properties. Geochim. Cosmochim. Acta 71, 1249–1265.

Guillot, B., Sator, N., 2007b. A computer simulation study of natural silicate melts. Part II: high pressure properties. Geochim. Cosmochim. Acta 71, 4538–4556.

Guillot, B., Sator, N., 2011. Carbon dioxide in silicate melts: a molecular dynamics simulation study. Geochim. Cosmochim. Acta 75, 1829–1857.

Hartwigsen, C., Goedecker, S., Hutter, J., 1998. Relativistic separable dual-space gaussian pseudopotentials from H to Rn. Phys. Rev. B 58, 3641–3662.

Hiet, J., 2009. Motifs structuraux dans des verres modèles pour le stockage des actinides. (Ph.D thesis). University of Orléans, p. 354.

Hiet, J., Deschamps, M., Pellerin, N., Fayon, F., Massiot, D., 2009. Probing chemical disorder in glasses using silicon-29 NMR spectral editing. Phys. Chem. Chem. Phys. 11, 6935–6940.

Holloway, J.R., 1981. Volatile interactions in magmas. In: Newton, R.C., Navrotsky, A., Wood, B.J. (Eds.), Thermodynamics of Melts and Minerals (Advances in Physical Geochemistry I). Springer-Verlag, New York, pp. 273–293.

Iacono-Marziano, G., Gaillard, F., Pichavant, M., 2008. Limestone assimilation by basaltic magmas: an experimental re-assessment and application to Italian volcanoes. Contrib. Mineral. Petrol. 155, 719–738.

Iacono-Marziano, G., Morizet, Y., Le Trong, E., Gaillard, F., 2012. New experimental data and semi-empirical parameterization of H_2O–CO_2 solubility in mafic melts. Geochim. Cosmochim. Acta 97, 1–23.

Jakobsson, S., 1997. Solubility of water and carbon dioxide in an icelandite at 1400 °C and 10 kilobars. Contrib. Mineral. Petrol. 127, 129–135.

Jambon, A., 1994. Earth degassing and large-scale geochemical cycling of volatile elements. In: Carroll, M.R., Holloway, J.R. (Eds.), Volatiles in Magmas (Reviews in Mineralogy). 30. Mineral. Soc. Am., Washington, DC, pp. 479–517.

Karki, B.B., Stixrude, L.P., 2010. Viscosity of $MgSiO_3$ liquid at Earth's mantle conditions: implications for an early magma ocean. Science 328, 740.

Kohn, S.C., Brooker, R.A., Dupree, R., 1991. ^{13}C MAS NMR: a method for studying CO_2 speciation in glasses. Geochim. Cosmochim. Acta 55, 3879–3884.

Krack, M., 2005. Pseudopotentials for H to Kr optimized for gradient-corrected exchange-correlation functionals. Theor. Chem. Accounts 114, 145–152.

Le Losq, C., Neuville, D.R., Florian, P., Henderson, G.S., Massiot, D., 2014. The role of Al^{3+} on rheology and structural changes in sodium silicate and aluminosilicate glasses and melts. Geochim. Cosmochim. Acta 126, 495–517.

Lee, S.K., 2010. Effect of pressure on structure of oxide glasses at high pressure: insights from solid-state NMR of quadrupolar nuclides. Solid State Nucl. Magn. Reson. 38, 45–57.

Lee, S.K., 2011. Simplicity in melt densification in multicomponent magmatic reservoirs in Earth's interior revealed by multinuclear magnetic resonance. Proc. Natl. Acad. Sci. U. S. A. 108, 6847–6852.

Lee, S.K., Stebbins, J.F., 1999. The degree of aluminium avoidance in aluminosilicate glasses. Am. Mineral. 84, 937–945.

Lee, S.K., Stebbins, J.F., 2000. Al–O–Al and Si–O–Si sites in framework aluminosilicate glasses with Si/Al = 1: quantification of framework disorder. J. Non Cryst. Solids 270, 260–264.

Lee, C., Yang, W., Parr, R., 1988. Development of the Colle–Salvetti correlation-energy formula into a functional of the electron-density. Phys. Rev. B 37, 785–789.

Lee, S.K., Park, S.Y., Kim, H.-I., Tschauner, O., Asimow, P., Bai, L., Xiao, Y., Chow, P., 2012. Structure of shock compressed model basaltic glass: Insights from O K-edge X-ray Raman scattering and high-resolution ^{27}Al NMR spectroscopy. Geophys. Res. Lett. 39. http://dx.doi.org/10.1029/2012GL050861.

Lesne, P., Scaillet, B., Pichavant, M., Beny, J.M., 2011. The carbon dioxide solubility in alkali basalts: an experimental study. Contrib. Mineral. Petrol. 162, 153–168. http://dx.doi.org/10.1007/s00410-010-0585-0.

Lippert, G., Hutter, J., Parrinello, M., 1997. A hybrid Gaussian and plane wave density functional scheme. Mol. Phys. 92, 477–487.

Lippmaa, E., Mägi, M., Samoson, A., Engelhardt, G., Grimmer, A.-R., 1980. Structural studies of silicates by solid-state high-resolution ^{29}Si NMR. J. Am. Chem. Soc. 102, 4889–4893.

Maekawa, H., Yokokawa, T., 1997. Effects of temperature on silicate melt structure: a high temperature ^{29}Si NMR study of $Na_2Si_2O_5$. Geochim. Cosmochim. Acta 61, 2569–2575.

Maekawa, H., Maekawa, T., Kawamura, K., Yokokawa, T., 1991. The structural groups of alkali silicate glasses determined from ^{29}Si MAS NMR. J. Non-Cryst. Solids 127, 53–64.

Malfait, W.J., Halter, W.E., Morizet, Y., Meier, B.H., Verel, R., 2007a. Structural control on bulk melt properties: single and double quantum ^{29}Si NMR spectroscopy on alkali–silicate glasses. Geochim. Cosmochim. Acta 71, 6002–6018.

Malfait, W.J., Zakaznova-Herzog, V.P., Halter, W.E., 2007b. Quantitative Raman spectroscopy: high-temperature speciation of potassium silicate melts. J. Non-Cryst. Solids 353, 4029–4042.

Malfait, W.J., Seifert, R., Sanchez-Valle, C., 2014. Densified glasses as structural proxies for high-pressure melts: configurational compressibility of silicate melts retained in quenched and decompressed glasses. Am. Mineral. 99, 2142–2145.

Massiot, D., Fayon, F., Capron, M., King, I., Le Calvé, S., Alonso, B., Durand, J.-O., Bujoli, B., Gan, Z., Hoatson, G., 2002. Modelling one and two-dimensional solid-state NMR spectra. Magn. Reson. Chem. 40, 70–76.

Massuyeau, M., Gardés, E., Morizet, Y., Gaillard, F., 2015. The transition from carbonate to silicate liquids during the partial melting of carbonated peridotite, modelled by the activity of silica. (submitted for publication), Chem. Geol. (in this issue).

McDade, P., Wood, B.J., Van Westrenen, W., Brooker, R.A., Gudmundsson, G., Soulard, H., Najorka, J., Blundy, J., 2002. Pressure corrections for a selection of piston–cylinder cell assemblies. Min. Mag. 66, 1021–1028.

McMillan, P.F., Poe, B.T., Gillet, P., Reynard, B., 1994. A study of SiO_2 glass and supercooled liquid to 1950 K via a high-temperature Raman spectroscopy. Geochim. Cosmochim. Acta 58, 3653–3664.

Merzbacher, C.I., Sherriff, B.L., Hartman, J.S., White, W.B., 1990. A high-resolution ^{29}Si and ^{27}Al NMR study of alkaline earth aluminosilicate glasses. J. Non-Cryst. Solids 124, 194–206.

Morizet, Y., Kohn, S.C., Brooker, R.A., 2001. Annealing experiments on CO_2-bearing jadeite glass: an insight into the true temperature dependence of CO_2 speciation in silicate melts. Min. Mag. 65, 701–707.

Morizet, Y., Brooker, R.A., Kohn, S.C., 2002. CO_2 in haplo-phonolite melt: solubility, speciation and carbonate complexation. Geochim. Cosmochim. Acta 66, 1809–1820.

Morizet, Y., Paris, M., Gaillard, F., Scaillet, B., 2010. C–O–H fluid solubility in haplobasalt under reducing conditions: an experimental study. Chem. Geol. 279, 1–16.

Morizet, Y., Brooker, R.A., Iacono-Marziano, G., Kjarsgaard, B., 2013a. Quantification of CO_2 dissolved in silicate glasses of various compositions with micro-Raman spectroscopy. Am. Mineral. 98, 1788–1802.

Morizet, Y., Paris, M., Di Carlo, I., Scaillet, B., 2013b. Effect of sulphur on the structure of silicate melts under oxidizing conditions. Chem. Geol. 358, 131–147.

Morizet, Y., Paris, M., Gaillard, F., Scaillet, B., 2014a. Carbon dioxide in silica-undersaturated melt. Part I: the effect of mixed alkalis (K and Na) on CO_2 solubility and speciation. Geochim. Cosmochim. Acta 141, 45–61.

Morizet, Y., Paris, M., Gaillard, F., Scaillet, B., 2014b. Carbon dioxide in silica-undersaturated melt. Part II: effect of CO_2 on quenched glass structure. Geochim. Cosmochim. Acta 144, 202–216.

Moynihan, C.T., Easteal, A.J., DeBolt, M.A., Tucker, J., 1976. Dependence of fictive temperature of glass on cooling rate. J. Am. Ceram. Soc. 59, 12–16.

Mysen, B.O., 1988. Structure and properties of silicate melts. Development in Geochemistry vol. 4. Elsevier, Amsterdam (354 pp.).

Mysen, B.O., 1990. Effect of pressure, temperature and bulk composition on the structure and species distribution in depolymerised alkali aluminosilicate melts and quenched melts. J. Geophys. Res. B 95, 15733–15744.

Mysen, B.O., 1997. Aluminosilicate melts: structure, composition and temperature. Contrib. Mineral. Petrol. 127, 104–118.

Mysen, B.O., 2012. Silicate–COH melt and fluid structure, their physicochemical properties, and partitioning of nominally refractory oxides between melts and fluids. Lithos 148, 228–246.

Mysen, B.O., 2013. Structure–property relationships of COHN-saturated silicate melt coexisting with COHN fluid: a review of in-situ, high-temperature, high-pressure experiments. Chem. Geol. 346, 113–124.

Mysen, B.O., Cody, G.D., 2005. Solution mechanisms of H_2O in depolymerized peralkaline melts. Geochim. Cosmochim. Acta 69, 5557–5566.

Mysen, B.O., Frantz, J.D., 1994. Silicate melts at magmatic temperatures: in-situ structure determination to 1651 °C and effect of temperature and bulk composition on the mixing behavior of structural units. Contrib. Mineral. Petrol. 117, 1–14.

Mysen, B.O., Richet, P., 2005. Silicate Glasses and Melts: Properties and Structure. p. 560.

Mysen, B.O., Virgo, D., Scarfe, C.M., 1980. Relations between the anionic structure and viscosity of silicate melts - A Raman spectroscopic study. Am. Mineral. 65, 690–710.

Mysen, B.O., Virgo, D., 1980. Solubility mechanisms of carbon dioxide in silicate melts: a Raman spectroscopic study. Am. Mineral. 65, 885–899.

Mysen, B.O., Yamashita, S., 2010. Speciation of reduced C–O–H volatiles in coexisting fluids and silicate melts determined in-situ to ~1.4 GPa and 800 °C. Geochim. Cosmochim. Acta 74, 4577–4588.

Neuville, D.R., Mysen, B.O., 1996. Role of the Al in the silicate network: in situ, high temperature study of glasses and melts on the join SiO_2–$NaAlO_2$. Geochim. Cosmochim. Acta 60 (10), 1727–1737.

Neuville, D.R., Cormier, L., Massiot, D., 2006. Al coordination and speciation in calcium aluminosilicate glasses: effects of composition determined by ^{27}Al MQ-MAS NMR and Raman spectroscopy. Chem. Geol. 229, 173–185.

Newman, S., Lowenstern, J.B., 2002. VOLATILECALC: a silicate melt–H_2O–CO_2 solution model written in Visual Basic for Excel, source. Comput. Geosci. 28, 597–604.

Nosé, S., 1984a. A molecular-dynamics method for simulations in the canonical ensemble. Mol. Phys. 52, 255–268.

Nosé, S., 1984b. A unified formulation of the constant temperature molecular-dynamics methods. J. Chem. Phys. 81, 511–519.

Nowak, M., Porbatzki, D., Spickenbom, K., Diedrich, O., 2003. Carbon dioxide speciation in silicate melts: a restart. Earth Planet. Sci. Lett. 207, 131–139.

Ohlhorst, S., Behrens, H., Holts, F., 2001. Compositional dependence of molar absorptivities of near-infrared OH^- and H_2O bands in rhyolitic to basaltic glasses. Chem. Geol. 174, 5–20.

Pan, V., Holloway, J.R., Hervig, R., 1991. The pressure and temperature dependence of carbon dioxide solubility in tholeiitic basalt melts. Geochim. Cosmochim. Acta 55, 1587–1595.

Papale, P., 1999. Modeling of the solubility of a two-component H_2O + CO_2 fluid in silicate liquids. Am. Mineral. 84, 477–492.

Pawley, A.R., Holloway, J.R., McMillan, P.F., 1992. The effect of oxygen fugacity on the solubility of carbon–oxygen fluids in basaltic melt. Earth Planet. Sci. Lett. 110, 213–225.

Sanloup, C., Drewitt, J.W.E., Konôpková, Z., Dalladay-Simpson, P., Morton, D.M., Nachiketa, R., van Westrenen, W., Morgenroth, W., 2013. Structural change in molten basalt at deep mantle conditions. Nature 503, 104–107.

Schmidt, B.C., Riemer, T., Kohn, S.C., Behrens, H., Dupree, R., 2000. Different water solubility mechanisms in hydrous glasses along the Qz–Ab Join: evidence from NMR spectroscopy. Geochim. Cosmochim. Acta 64, 513–526.

Schneider, J., Mastelaro, V.R., Zanotto, E.D., Shakhmatkin, B.A., Vedishcheva, N.M., Wright, A.C., Panepucci, H., 2003. Q^n distribution in stoichiometric silicate glasses: thermodynamic calculations and ^{29}Si high resolution NMR measurements. J. Non-Cryst. Solids 325, 164–178.

Schramm, C.M., De Jong, B.H.W.S., Parziale, V.E., 1984. ^{29}Si magic angle spinning NMR study on local silicon environments in amorphous and crystalline lithium silicates. J. Am. Chem. Soc. 106, 4396–4402.

Seifert, R., Malfait, W.J., Lerch, P., Sachez-Valle, C., 2013. Partialmolar volume and compressibility of dissolved CO_2 in glasseswith magmatic compositions. Chem. Geol. 358, 119–130.

Shishkina, T.A., Botcharnikov, R.E., Holtz, F., Almeev, R.R., Portnyagin, M.V., 2010. Solubility of H_2O- and CO_2-bearing fluids in tholeiitic basalts at pressures up to 500 MPa. Chem. Geol. 277, 115–125.

Spickenbom, K., Sierralra, M., Nowak, M., 2010. Carbon dioxide and argon diffusion in silicate melts: insights into the CO_2 speciation in magmas. Geochim. Cosmochim. Acta 74, 6541–6564.

Stebbins, J.F., 1995. Dynamics and structure of silicate and oxide melts. In: Stebbins, J.F., McMillan, P.F., Dingwell, D.B. (Eds.), Nuclear Magnetic Resonance studies (Reviews in Mineralogy) 32. Mineralogical Society of America, Geochemical Society, Washington, pp. 190–246.

Stebbins, J.F., Farnan, I., 1992. Effects of high temperature on silicate liquid structure: a multinuclear NMR study. Science 255, 586–589.

Stebbins, J.F., Poe, B.T., 1999. Pentacoordinate silicon in high-pressure crystalline and glassy phases of calcium disilicate ($CaSi_2O_5$). Geophys. Res. Lett. 26, 2521–2523.

Stebbins, J.F., Xue, X., 2014. NMR spectroscopy of inorganic Earth materials. In: Henderson, G.S., Neuville, D.R., Downs, R.T. (Eds.), Spectroscopic Methods in Mineralogy and Material Sciences (Reviews in Mineralogy and Geochemistry) 78. Mineral. Soc. Am., Washington, DC, pp. 605–653.

Stebbins, J.F., Kroeker, S., Lee, S.K., Kiczenski, T.J., 2000. Quantification of 5 and 6-coordinated Al ions in aluminosilicate and fluoride containing glasses by high field, high resolution ^{27}Al NMR. J. Non-Cryst. Solids 275, 1–6.

Stebbins, J.F., Dubinsky, E.V., Kanehashi, K., Kelsey, K.E., 2008. Temperature effects on non-bridging oxygen and aluminium coordination number in calcium aluminosilicate glasses and melts. Geochim. Cosmochim. Acta 72, 910–925.

Symonds, R.B., Rose, W.I., Bluth, G.J.S., Gerlach, T.M., 1994. Volcanic-gas studies: methods, results and applications. In: Carroll, M.R., Holloway, J.R. (Eds.), Volatiles in Magmas (Review in Mineralogy) 30. Mineral. Soc. Am., Washington, DC, pp. 1–66.

Thibault, Y., Holloway, J.R., 1994. Solubility of CO_2 in a Ca-rich leucitite: effects of pressure, temperature and oxygen fugacity. Contrib. Mineral. Petrol. 116, 216–224.

Thompson, L.M., Stebbins, J.F., 2013. Interaction between composition and temperature effects on non-bridging oxygen and high-coordinated aluminum in calcium aluminosilicate glasses. Am. Mineral. 98, 1980–1987.

Toplis, M.J., Kohn, S.C., Smith, M.E., Poplett, I.J.F., 2000. Fivefold-coordinated aluminium in tectosilicate glasses observed by triple quantum MAS NMR. Am. Mineral. 85, 1556–1560.

Tropin, T.V., Schmelzer, J.W.P., Schick, C., 2011. On the dependence of the properties of glasses on cooling and heating rates II Prigogine–Defay ratio, fictive temperature and fictive pressure. J. Non-Cryst. Solids 357, 1303–1309.

Truckenbrodt, J., Johannes, W., 1999. H_2O loss during piston–cylinder experiments. Am. Mineral. 84, 1333–1335.

VandeVondele, J., Hutter, J., 2007. Gaussian basis sets for accurate calculations on molecular systems in gas and condensed phases. J. Chem. Phys. 127, 114105.

VandeVondele, J., Krack, M., Mohamed, F., Parrinello, M., Chassaing, T., Hutter, J., 2005. Quickstep: Fast and accurate density functional calculations using a mixed gaussian and plane waves approach. Comput. Phys. Commun. 167, 103–128.

Vuilleumier, R., 2006. Density functional theory based ab initio molecular dynamics using the Car–Parrinello approach. In: Ferrario, M., Ciccotti, G., Binder, K., et al. (Eds.), Computer Simulations in Condensed Matter: From Materials to Chemical Biology (Lecture Notes in Physics). Springer (chapter 8).

Vuilleumier, R., Sator, N., Guillot, B., 2009. Computer modeling of natural silicate melts: what can we learn from ab initio simulations. Geochim. Cosmochim. Acta 73, 6313–6339.

Wallace, M.E., Green, D.H., 1988. An experimental determination of primary carbonatite magma composition. Nature 335, 343–346.

Webb, S., 1997. Silicate melts: relaxation, rheology, and the glass transition. Rev. Geophys. 35, 191–218.

Xue, X., Kanzaki, M., 2004. Dissolution mechanisms of water in depolymerised silicate melts: constraints from ^{1}H and ^{29}Si NMR spectroscopy and ab initio calculations. Geochim. Cosmochim. Acta 68, 5027–5057.

Zeng, Q., Nekvasil, H., Grey, C.P., 1999. Proton Environments in Hydrous Aluminosilicate Glasses: A TRAPDOR NMR Study. J. Phys. Chem B 103, 7406–7415.

Zeng, Q., Nekvasil, H., Grey, C.P., 2000. In support of a depolymerization model for water in sodium aluminosilicate glasses: Information from NMR spectroscopy. Geochim. Cosmochim. Acta 64, 883–896.

Zhang, P., Grandinetti, P.J., Stebbins, J.F., 1997. Anionic species determination in $CaSiO_3$ glass using two-dimensional ^{29}Si NMR. J. Phys. Chem. 101, 4004–4008.